Article

SOURCE DATA | TRANSPARENT PROCESS

THE EMBO JOURNAL

m^{6}A modification of HSATIII lncRNAs regulates temperature-dependent splicing

Kensuke Ninomiya[1,2], Junichi Iwakiri[3], Mahmoud Khamis Aly[2,4], Yuriko Sakaguchi[5], Shungo Adachi[6], Tohru Natsume[6], Goro Terai[3], Kiyoshi Asai[3], Tsutomu Suzuki[5] & Tetsuro Hirose[1,2,*]

Abstract

Nuclear stress bodies (nSBs) are nuclear membraneless organelles formed around stress-inducible HSATIII architectural long noncoding RNAs (lncRNAs). nSBs repress splicing of hundreds of introns during thermal stress recovery, which are partly regulated by CLK1 kinase phosphorylation of temperature-dependent Ser/Arg-rich splicing factors (SRSFs). Here, we report a distinct mechanism for this splicing repression through protein sequestration by nSBs. Comprehensive identification of RNA-binding proteins revealed HSATIII association with proteins related to N^6-methyladenosine (m^{6}A) RNA modification. 11% of the first adenosine in the repetitive HSATIII sequence were m^{6}A-modified. nSBs sequester the m^{6}A writer complex to methylate HSATIII, leading to subsequent sequestration of the nuclear m^{6}A reader, YTHDC1. Sequestration of these factors from the nucleoplasm represses m^{6}A modification of pre-mRNAs, leading to repression of m^{6}A-dependent splicing during stress recovery phase. Thus, nSBs serve as a common platform for regulation of temperature-dependent splicing through dual mechanisms employing two distinct ribonucleoprotein modules with partially m^{6}A-modified architectural lncRNAs.

Keywords long noncoding RNA; m^{6}A modification; molecular sponge; nuclear stress bodies; pre-mRNA splicing

Subject Categories Chromatin, Transcription & Genomics; RNA Biology

DOI 10.15252/embj.2021107976 | Received 9 February 2021 | Revised 24 May 2021 | Accepted 28 May 2021 | Published online 29 June 2021

The EMBO Journal (2021) 40: e107976

Introduction

Long noncoding RNAs (lncRNAs) have recently been recognized as fundamental regulators of eukaryotic gene expression, but their mechanisms of action remain largely unknown. A subset of lncRNAs, termed architectural lncRNAs, function in a variety of eukaryotes as structural scaffolds in nuclear bodies, which are membraneless subnuclear organelles (Kopp & Mendell, 2018; Hirose, Yamazaki *et al*, 2019; Yamazaki, Nakagawa *et al*, 2019). Nuclear bodies are large biomolecular condensates usually located in inter-chromatin spaces in the nucleoplasm. The architectural lncRNAs sequester specific sets of RNA-binding proteins, which likely causes demixing to form nuclear bodies. These nuclear bodies play key roles in a number of nuclear processes, including sequestration of biomolecules and formation of organizational hubs to coordinate specific biochemical reactions and macromolecular assembly (Shin & Brangwynne, 2017).

Nuclear stress bodies (nSBs) are the nuclear bodies formed during thermal stress exposure. nSB formation depends on HSATIII architectural lncRNAs, which are transcribed upon thermal stress from the primate-specific pericentromeric satellite III regions on several chromosomes (Biamonti & Vourc'h, 2010). HSATIII lncRNAs consist mostly of GGAAU repeat sequences which recruit specific sets of RNA-binding proteins to form nSBs (Biamonti & Vourc'h, 2010). Under thermal stress conditions, nSBs selectively sequester various Ser/Arg (SR)-rich splicing factors (SRSFs), such as SRSF1 and SRSF9, and SR-related proteins, such as TRA2B, which indicate regulatory roles of nSBs in pre-mRNA splicing during thermal stress. Our recent transcriptomic analysis in HSATIII-depleted HeLa cells revealed that HSATIII lncRNAs (and nSBs) promote retention of 533 introns during the stress recovery stage, which was consistent with the hypothesis that temperature-dependent splicing events are regulated by SRSFs sequestered in nSBs (Ninomiya *et al*, 2020). SRSFs are globally dephosphorylated under thermal stress conditions and re-phosphorylated after stress removal (Guil & Caceres, 2007). We found that nSBs accelerate the rate of SRSF9 rephosphorylation by recruiting CDC-like kinase 1 (CLK1) specifically after stress removal (Ninomiya, Adachi *et al*, 2020). Consequently, the re-phosphorylated SRSF9 promotes intron retention of the target pre-mRNAs. Thus, nSBs act as a reaction crucible for SRSF9 phosphorylation to properly control temperature-dependent splicing. The SRSF9/CLK1-dependent mechanism regulates retention of only a subset of the HSATIII-target introns. This raises the possibility that nSBs confer distinct mechanism(s) to regulate retention of the remaining target introns.

1 Graduate School of Frontier Biosciences, Osaka University, Suita, Japan
2 Institute for Genetic Medicine, Hokkaido University, Sapporo, Japan
3 Graduate School of Frontier Sciences, University of Tokyo, Kashiwa, Japan
4 Faculty of Biotechnology, Modern Sciences and Arts University, Giza, Egypt
5 Graduate School of Engineering, The University of Tokyo, Tokyo, Japan
6 Cellular and Molecular Biotechnology Research Institute, National Institute for Advanced Industrial Science and Technology (AIST), Tokyo, Japan
*Corresponding author. Tel: +81 6 6879 4674, E-mail: hirose@fbs.osaka-u.ac.jp

N^6-methyladenosine (m^6A) is one of the most abundant internal RNA modifications in eukaryotic mRNAs and lncRNAs. m^6A affects the whole process of RNA metabolism, including transcription, pre-mRNA splicing, nuclear RNA export, RNA stabilization, and translation (Shi, Wei *et al*, 2019; Zaccara, Ries *et al*, 2019). m^6A is introduced by an m^6A writer complex consisting of the catalytic subunit, methyltransferase-like 3 (METTL3) (Bokar, Shambaugh *et al*, 1997; Liu, Yue *et al*, 2014), the substrate-recognizing subunit METTL14 (Sledz & Jinek, 2016; Wang, Doxtader *et al*, 2016; Wang, Feng *et al*, 2016; Delaunay & Frye, 2019), Wilms tumor 1-associated protein (WTAP) (Zhong, Li *et al*, 2008; Ping, Sun *et al*, 2014), KIAA1429 (Schwartz, Mumbach *et al*, 2014), ZC3H13 (Wen, Lv *et al*, 2018), RNA binding motif protein 15 (RBM15), and the RBM15 paralog SPEN (Moindrot, Cerase *et al*, 2015; Patil, Chen *et al*, 2016; Yang, Hsu *et al*, 2018). The consensus sequence motif for m^6A modification by the METTL3/14 writer complex is GRm^6ACH (R is A or G, H is not G) and is commonly GGm^6ACU (Schibler, Kelley *et al*, 1977). m^6A-modified RNAs are recognized by m^6A reader proteins, such as YT521-B homology (YTH) domain family members, YTHDC1 (Patil *et al*, 2016; Xiao, Adhikari *et al*, 2016), YTHDF1 (Wang, Zhao *et al*, 2015), YTHDF2 (Wang, Lu *et al*, 2014; Zhou, Wan *et al*, 2015; Du, Zhao *et al*, 2016), and YTHDF3 (Li, Chen *et al*, 2017; Shi, Wang *et al*, 2017), and specific heterogeneous nuclear ribonucleoproteins (HNRNPs) including HNRNPA2/B1 and HNRNPG (Alarcon, Goodarzi *et al*, 2015; Zhou, Shi *et al*, 2019). The m^6A reader proteins recruit other RNA-processing factor(s) to the m^6A-modified RNAs or influence the RNA secondary structure to regulate RNA processing and metabolism (Knuckles & Buhler, 2018). In mammalian cell nuclei, a nuclear m^6A reader protein, YTHDC1, is involved in various nuclear events, including regulation of splicing, processing, and stability of mRNAs, and specific lncRNA functions. In splicing regulation, YTHDC1 recruits SRSF3 to the m^6A-modified exonic splicing enhancer (ESE) to regulate splicing of adjacent introns (Xiao *et al*, 2016). The lncRNA, XIST, which mediates the transcriptional silencing of genes on the inactive X chromosome, is highly m^6A-modified. YTHDC1 recognition of these m^6A sites is required for XIST function through an unknown mechanism (Patil *et al*, 2016).

In this study, we show that HSATIII lncRNAs are highly m^6A modified by the m^6A writer complex, which is recruited to nSBs mainly during thermal stress recovery and leads to the sequestration of the nuclear m^6A reader protein, YTHDC1. This sequestration by nSBs diminishes the nucleoplasmic level of YTHDC1, resulting in m^6A-dependent splicing of the subset of HSATIII-target introns that is not regulated by the SRSF9/CLK1-mediated nSB functional pathway. We show that the GGAAU repeat sequence can preferentially interact with both SRSF9- and m^6A-related factors; unmodified GGAAU selects SRSF9 while m^6A-modified GGAAU selects YTHDC1 to form the distinct ribonucleoprotein complexes. Therefore, we argue that nSBs serve as both a molecular sponge to sequester m^6A-related factors and a reaction crucible for SRSF9 phosphorylation. These mechanisms cooperatively control intron retention during thermal stress recovery and are enacted by the presence of partially m^6A-modified HSATIII lncRNAs.

Results

m^6A-RNA modification factors are localized in nSBs

Our comprehensive identification of HSATIII lncRNA-binding proteins by mass spectrometry (ChIRP-MS) analysis identified 141 nSB candidate proteins (Ninomiya *et al*, 2020). Among them, we recognized a number of proteins related to m^6A-RNA modification, such as components of the m^6A writer complex, KIAA1429, ZC3H13, RBM15, RBM15B, SPEN, and WTAP, and the nuclear m^6A reader protein, YTHDC1 (Fig 1A). To confirm the nSB localization of the m^6A factors, we performed immunofluorescence (IF) staining of WTAP, KIAA1429, and YTHDC1 combined with HSATIII-fluorescent *in situ* hybridization (FISH). In thermal stress-exposed HeLa cells (42°C for 2 h followed by 37°C recovery for 1 h), the immuno-positive granules of these proteins overlapped with HSATIII but were dispersed throughout the nucleoplasm upon HSATIII knockdown (KD), indicating their localization in nSBs (Figs 1B and C and EV1A). Moreover, immunostaining using an anti-m^6A antibody revealed the presence of m^6A-modified RNA (m^6A-RNA) in nSBs (Fig 1D). We also confirmed that treatment of

Figure 1. Localization of m^6A factors within nSBs.

A m^6A-related proteins identified by HSATIII-ChIRP-MS (*cf.* table EV3 in Ninomiya *et al*, 2020).

B, C HSATIII lncRNA-dependent localization of m^6A-related factors. Control and HSATIII knockdown HeLa cells were exposed to thermal stress (42°C for 2 h and recovery for 1 h at 37°C) and stained by HSATIII-FISH and immunofluorescence using an anti-WTAP antibody (B) or anti-YTHDC1 antibody (C). The nuclei were stained with DAPI. Scale bar: 10 μm.

D Enrichment of m^6A-RNAs in nSBs. Thermal stress-exposed HeLa cells were stained by HSATIII-FISH and immunofluorescence using an anti-m^6A antibody. The nuclei were stained with DAPI. Scale bar: 10 μm.

E–G 3-DZA inhibits localization of m^6A-RNAs (E), YTHDC1 (F), and WTAP (G) in nSBs. HeLa cells were exposed to thermal stress in the presence of 3-DZA (100 μM) and stained as described above. Scale bar: 10 μm.

H–J Box plot of relative intensities of m^6A (H), YTHDC1 (I), and WTAP (J) to HSATIII within nSBs in individual nuclei. nSB areas were defined by binarized images of HSATIII-FISH. The mean is indicated with X. The first and third quartiles are the ends of the box, the median is indicated with a vertical line in the box, and the minimum and maximum except for the outliers are the ends of the whiskers. The outliers are indicated with open circles. *P*-value (Mann–Whitney U-test) is shown above ($n = 30$).

K YTHDC1 accumulation within nSBs was arrested by METTL3 knockdown. HeLa cells were stained as described in Fig 1C. Scale bar: 10 μm.

L Box plot of relative intensities of YTHDC1 to HSATIII within nSBs in individual nuclei ($n = 30$). The mean is indicated with X. The first and third quartiles are the ends of the box, the median is indicated with a vertical line in the box, and the minimum and maximum except for the outliers are the ends of the whiskers. The outliers are indicated with open circles. *P*-values (Kruskal–Wallis test, followed by Dunn's multiple comparison test) are shown above.

Source data are available online for this figure.

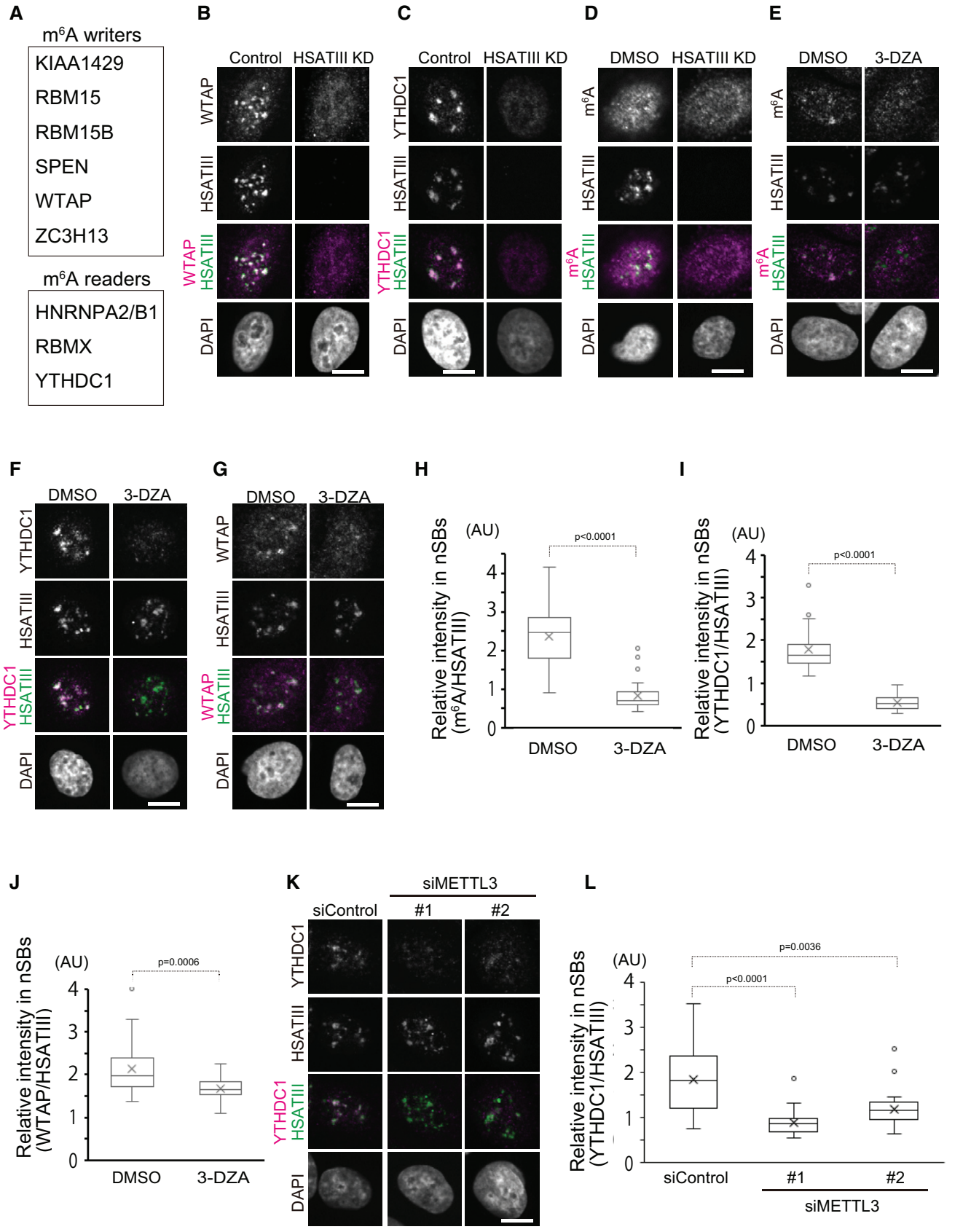

Figure 1.

cells with a global methylase inhibitor, 3-deazaadenosine (3-DZA), mostly abolished the m^{6}A-RNA and YTHDC1 signals in nSBs and even diminished WTAP signals without affecting nSB integrity (Fig 1E–J). 3-DZA treatment did not impair recruitment of scaffold attachment factor B (SAFB), an m^{6}A-unrelated nSB component (Fig EV1B and C), nor affect the steady-state levels of YTHDC1 and WTAP (Fig EV1D and E), indicating that 3-DZA impaired m^{6}A methylation of nSB-localized RNAs and the concomitant recruitment of YTHDC1 into nSBs. It remains unexplained how recruitment of WTAP as a component of the m^{6}A writer complex by nSBs was impaired by methylase inhibition. Coincidently, the mobility of WTAP upon SDS–PAGE was slightly decreased by 3-DZA treatment, probably because of post-translational modification of WTAP (Fig EV1D), and this might be related to its nSB recruitment. Our attempts to detect METTL3 and METTL14 as the catalytic core of the m^{6}A writer complex by IF were unsuccessful probably because of their lower stability in the complexes or lower antibody quality. However, METTL3 KD using two siRNAs, which concomitantly decreased METTL14 levels (Fig EV1F), impaired YTHDC1 recruitment and m^{6}A enrichment into nSBs (Figs 1K and L, and EV1G and F). These results collectively indicate that nSB-localized RNAs are methylated by the canonical m^{6}A writer complex with METTL3/14 and that YTHDC1 is concomitantly associated with m^{6}A-RNAs in nSBs.

HSATIII lncRNAs are m^{6}A-modified in nSBs

To examine whether HSATIII lncRNAs themselves are m^{6}A-modified, we purified HSATIII lncRNAs from thermal stress-treated HeLa cells and analyzed their RNA modifications by RNA mass spectrometry (RNA-MS) (Fig 2A). To obtain highly purified HSATIII lncRNAs, the HSATIII ribonucleoprotein complexes were purified by HSATIII-ChIRP using magnetic beads conjugated with biotinylated HSATIII antisense oligonucleotides (ASOs) (Ninomiya *et al*, 2020). We then further purified HSATIII lncRNA from the RNAs prepared from the first ChIRP fraction with the same ASO beads. U1 snRNA, which is localized in nSBs (Metz, Soret *et al*, 2004), was detected in the first HSATIII-ChIRP fraction (Fig 2B, lane 2) but not in the second HSATIII-purified fraction (Fig 2B, lane 4, 5). The purified HSATIII RNAs were digested by ribonuclease T1 and then subjected to RNA-MS analysis (Fig 2C–E). Among complex mixture of RNA fragments, we clearly detected AAUGp tetramer which is derived from the major repetitive sequence of HSATIII lncRNAs (Fig 2C). The sequence of this fragment was confirmed by collision-induced dissociation (CID) (Fig 2D). In addition, we also detected the same tetramers with one or two methyl groups (Fig 2C). The CID analyses revealed that they are m^{6}AAUG and m^{6}Am^{6}AUG (approximately 7% and 4% of all AAUG fragments, respectively) (Fig 2C and D). To determine the species of the methyl modification, we performed LC/MS nucleoside analysis of the purified HSATIII RNAs and detected m^{6}A nucleoside as a major modification in HSATIII RNAs (Fig 2E). Taken together, these data indicate that the first adenosine of the repetitive GGAAU sequence in HSATIII lncRNAs is modified with m^{6}A at an approximate frequency of 11%, while the second adenosine is m^{6}A modified with about 4%. We also confirmed that cellular HSATIII lncRNAs were precipitated by the anti-m^{6}A antibody, which was significantly impaired by WTAP KD (Fig EV2A–C). These results indicate that specific adenosines in the repetitive sequence of HSATIII lncRNAs are m^{6}A-modified and that the methylation is likely deposited by the m^{6}A writer complex recruited to nSBs during thermal stress recovery.

m^{6}A-related factors are recruited to nSBs mainly during thermal stress recovery

To investigate temporal and environmental effects on the recruitment of m^{6}A-related factors to nSBs, we performed HSATIII-ChIRP-MS at various time points of thermal stress and recovery. As we previously reported (Ninomiya & Hirose, 2020; Ninomiya *et al*, 2020), HSATIII consists mostly of short-tandem repeat sequences; therefore, a single ChIRP probe against the HSATIII repeat sequence can efficiently capture entire RNP complexes, presumably through multivalent hybridization with unmasked regions of HSATIII lncRNAs. Accordingly, we counted MS-detected peptide numbers derived from each m^{6}A-related factor (Fig 3A and B and Dataset EV1). The recruitment of m^{6}A writer complex components, such as KIAA1429, RBM15, RBM15B, SPEN, WTAP, and ZC3H13, and the m^{6}A reader protein, YTHDC1, peaked at the early recovery time point of 1 h at 37°C, whereas the recruitment of SAFB, SRSF1, and SRSF9 reached maximum levels during thermal stress at 42°C for 2 h and gradually declined after stress removal (Fig 3B and Dataset EV1). ChIRP Western blotting also confirmed enrichment of the m^{6}A factors, especially during stress recovery (Fig 3C). We also monitored the temporal and temperature-dependent recruitment of

Figure 2. Specific m^{6}A modifications of HSATIII lncRNAs.

A Outline of the purification of HSATIII-derived AAUG fragments for RNA-MS analysis. HSATIII lncRNA is represented by magenta lines, and other nSB-localized RNAs, such as U1 snRNA, are represented by gray lines. Lane numbers in B are indicated by red text.

B Semi-quantitative RT–PCR validation of the purity of HSATIII lncRNAs. Purified RNAs at each step in A were validated by semi-quantitative RT-PCR. ChIRP using control oligonucleotide was performed as negative control (lane 3). U1 snRNA was examined as an nSB-localized non-HSATIII RNA. RT(-) samples (lanes 6–10) were used as negative controls for PCR without reverse transcription. Input: 10%.

C RNA-MS analysis of HSATIII lncRNAs digested by RNase T_1. Base peak chromatogram (BPC, top panel) and extracted chromatograms (XIC, lower panels) for the RNase T_1-digested fragments of the isolated HSATIII lncRNAs. XICs detecting for the negatively charged ions of AAUGp tetramer without modification (second panel), with one methylation (third panel), and two methylations (bottom panel). The sequence, mass-to-charge ratio (m/z), and charge state are indicated. NL; normalization level.

D Collision-induced dissociation spectra of AAUGp, m^{6}AAUGp, and m^{6}Am^{6}AUGp. The product ions are assigned as indicated.

E LC/MS single nucleoside analysis of the purified HSATIII lncRNAs. Proton adduct of m^{6}A nucleoside (*m/z* 282) is abundantly detected in UV trace at 260 nm (upper panel) as well as in extracted mass chromatogram (lower panel). The base ion (*m/z* 150.077) of m^{6}A nucleoside (*m/z* 282.119) is produced spontaneously by cleavage of the N-glycoside linkage during electrospray ionization (inserted mass spectrum).

Source data are available online for this figure.

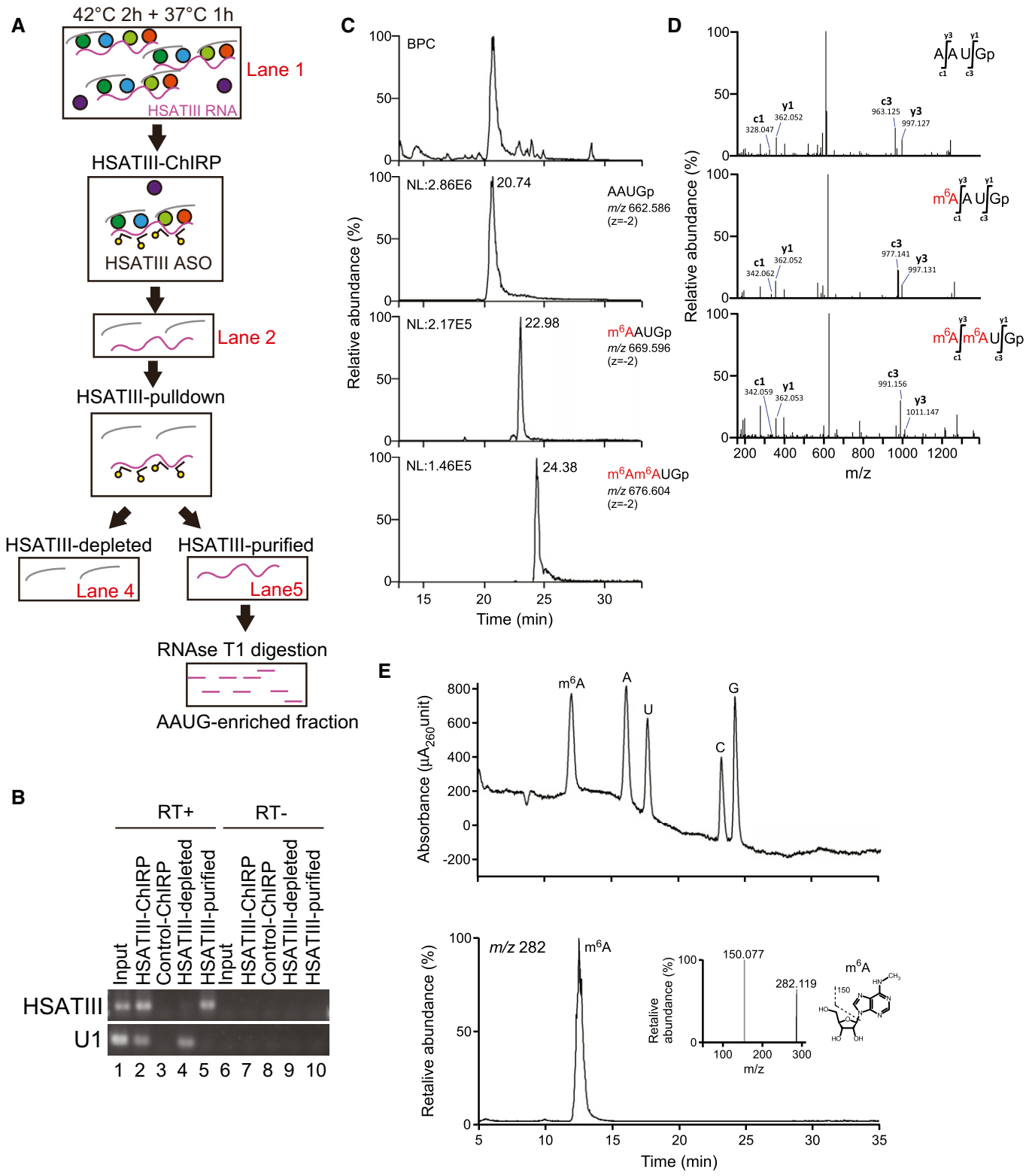

Figure 2.

m^{6}A-related factors in nSBs by IF combined with HSATIII-FISH. WTAP recruitment to nSBs was detectable at a low level during thermal stress but sharply increased at 1 h after stress removal (Fig 3D and E), whereas YTHDC1 was also mainly recruited after stress removal and remained in nSBs for at least 4 h after stress removal (Fig 3F and G). This is mostly consistent with the ChIRP result (Fig 3B and C, Dataset EV1). These results indicate that the m^{6}A writer complex is transiently recruited to nSBs after sensing the

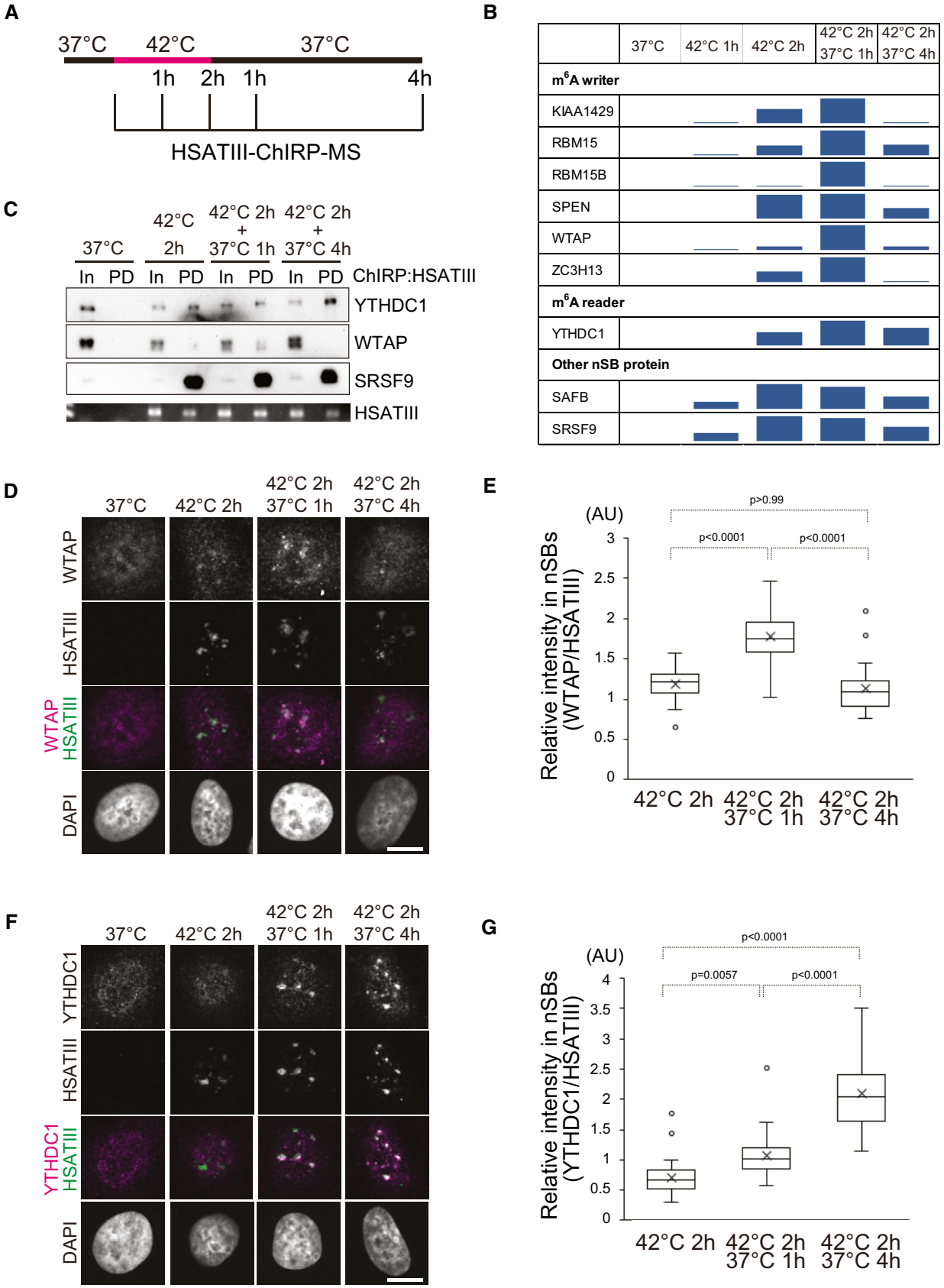

Figure 3.

Figure 3. Localization of the m^{6}A-related factors in nSBs during stress recovery.

A Schematic of HSATIII-ChIRP-MS at various time points during and after thermal stress exposure.

B Bar graph of relative ChIRP-MS enrichment score. ChIRP-MS enrichment score for each protein was calculated as (the average number of identified peptides at each time point + 0.00001) / (the average number of identified peptides at 37°C + 0.00001) and normalized to the maximum value of each protein.

C Western blot validation of HSATIII-ChIRP. nSB proteins (YTHDC1, WTAP, and SRSF9) were detected by Western blotting using specific antibodies (input 1%). HSATIII lncRNAs were detected by semi-quantitative RT–PCR (input 100%). In; input, PD; pulldown by ChIRP.

D–G (D, F) Changes in nSB localization of m^{6}A-related factors at various time points during and after thermal stress exposure. HeLa cells were exposed to thermal stress (42°C for 2 h) and cultured at 37°C for the indicated periods. m^{6}A-related factors were visualized by HSATIII-FISH and IF using anti-WTAP antibody (D) or anti-YTHDC1 antibody (F). Nuclei were stained with DAPI. Scale bar: 10 μm. (E, G) Box plot of relative intensities of WTAP (D) and YTHDC1 (F) to HSATIII within nSB areas in individual nuclei. nSB areas were defined by binarized images of HSATIII-FISH. The mean is indicated with X. The first and third quartiles are the ends of the box, the median is indicated with a vertical line in the box, and the minimum and maximum except for the outliers are the ends of the whiskers. The outliers are indicated with open circles. *P*-values (Kruskal–Wallis test, followed by Dunn's multiple comparison test) are shown above (n = 30).

Source data are available online for this figure.

temperature shift to 37°C, whereas YTHDC1 is similarly recruited but persistently retained in nSBs for longer periods.

nSBs effectively sequester nucleoplasmic m^{6}A-related factors

To investigate whether sequestration of m^{6}A-related factors in nSBs effectively decreases their nucleoplasmic levels, the average intensity of YTHDC1 in non-nSBs nucleoplasmic areas in control and HSATIII KD cells at 1 h after thermal stress removal was determined. The average intensity of YTHDC1 in the nucleoplasm was significantly decreased in the presence of nSBs (Fig 4A). We also investigated the correlation of nSB occupancy of the whole nucleus with the intensity of YTHDC1 outside of nSBs in control cells and found significant negative correlation between them (Fig 4B). From these data, we argue that nSBs sequester nucleoplasmic YTHDC1 in a size-dependent manner. Similar to YTHDC1, the intensity of nucleoplasmic WTAP was also decreased in the presence of nSBs, even though there was no correlation with nSB size (Fig 4C and D). It should be noted that total protein levels of YTHDC1 and WTAP were hardly affected by HSATIII KD (Fig 4E and F), supporting our argument that HSATIII lncRNAs effectively sequester YTHDC1 and WTAP from the nucleoplasm. We further validated HSATIII lncRNA-dependent sequestration of nucleoplasmic YTHDC1 and WTAP at different time points during thermal stress and recovery (Fig 4G and H). In a comparison of control and HSATIII KD cells, HSATIII-dependent sequestration of YTHDC1 and WTAP was observed mainly in the post-stress recovery phase, in which the effect of HSATIII was more persistent on YTHDC1 than WTAP (Fig 4G and H). It should be noted that nucleoplasmic YTHDC1 decreased upon thermal stress and gradually recovered after stress removal in both control and HSATIII KD cells, probably because thermal stress caused global degradation and/or nuclear mislocalization.

nSBs control splicing through sequestration of nuclear m^{6}A reader, YTHDC1

We have reported that nSBs promote nuclear intron retention of > 400 target mRNAs, especially during recovery from thermal stress exposure (Ninomiya *et al*, 2020). We also found that nSBs accelerate CLK1-dependent rephosphorylation of SRSFs, which are responsible for regulating the splicing of a subset of target mRNAs (Ninomiya *et al*, 2020). The remaining target mRNAs were not affected by CLK1-dependent phosphorylation of SRSFs; therefore, we expected that nSBs control splicing through additional distinct mechanism(s). Considering that YTHDC1 as a nuclear m^{6}A reader protein impacts pre-mRNA splicing (Xiao *et al*, 2016), our data above raised the intriguing possibility that HSATIII lncRNAs, which themselves are highly m^{6}A-modified, control splicing by sequestrating YTHDC1 in nSBs. We reanalyzed the RNA sequencing (RNA-seq) data upon YTHDC1 KD reported by Yang group (Xiao *et al*, 2016), and subsequently compared them with our RNA-seq data from thermally

Figure 4. Sequestration of YTHDC1 and WTAP within nSBs.

A–D (A, C) Nucleoplasmic YTHDC1 (A) and WTAP (B) intensities upon HSATIII knockdown. Control and HSATIII knockdown cells after thermal stress exposure (42°C for 2 h and recovery for 1 h at 37°C) were stained by HSATIII-FISH and IF using anti-YTHDC1 or anti-WTAP antibodies. nSB and whole nuclear areas were defined by binarized images of HSATIII and DAPI, respectively. Box plots represent the average intensities of YTHDC1 and WTAP in the non-nSB nucleoplasm area of each nucleus. The first and third quartiles are the ends of the box, the median is indicated with a vertical line in the box, and the minimum and maximum except for the outliers are the ends of the whiskers. The outliers are indicated with open circles. The mean is indicated with X. *P*-value (Mann–Whitney U-test) is shown above (n = 40). (B, D) Correlation between the intensity of YTHDC1 (B) or WTAP (D) in non-nSB nucleoplasm and the nSB occupancy in individual nuclei. nSB occupancy is the ratio of the nSB area to the whole nuclear area of each nucleus in (A) and (C). Pearson coefficient of correlation (R) and *P*-value are shown above (n = 40).

E Western blot validation of WTAP and YTHDC1 protein levels after HSATIII knockdown. HeLa cells were transfected with HSATIII ASO and control sense oligonucleotide, cultured for 16 h, and exposed to thermal stress (42°C for 2 h and recovery for 1 h at 37°C). Cell extracts were used for Western blotting. GAPDH is a control.

F Quantification of E showing mean ± SD values (n = 3). *P*-values (Student's *t*-test) are shown above.

G, H HSATIII-dependent sequestration of nucleoplasmic YTHDC1 (G) and WTAP (H) at four time points during thermal stress and recovery. The experiments same as A and C were performed at the indicated timepoints. The mean is indicated with X. The first and third quartiles are the ends of the box, the median is indicated with a vertical line in the box, and the minimum and maximum except for the outliers are the ends of the whiskers. The outliers are indicated with open circles. *P*-values (Kruskal–Wallis test, followed by Dunn's multiple comparison test) are shown above (n = 40).

Source data are available online for this figure.

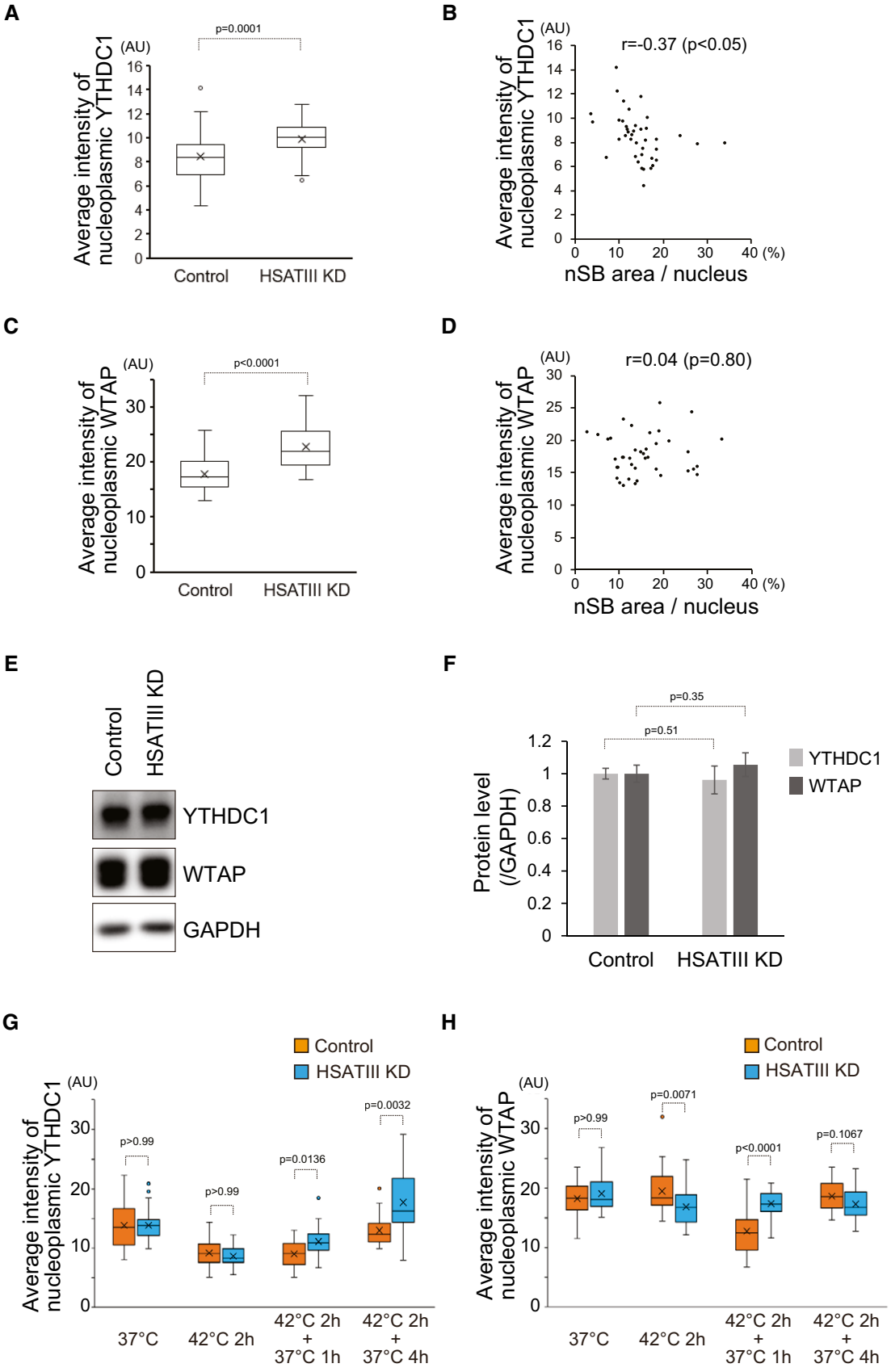

Figure 4.

stressed cells (Ninomiya *et al*, 2020). We identified that retention of 36 introns was promoted upon YTHDC1 KD. Furthermore, 14 of these 36 introns were included among the 533 retained introns controlled by HSATIII lncRNAs (HSATIII-target introns) (Ninomiya *et al*, 2020), indicating that YTHDC1 promotes splicing of a subset of HSATIII-target introns (Appendix Table S1). To more directly test the hypothesis that HSATIII lncRNAs promote intron retention through sequestration of YTHDC1, we searched for introns whose expression was up-regulated by YTHDC1 KD in HSATIII-depleted cells but less affected in HSATIII-expressing cells (Figs 5A and EV3A). We performed RNA-seq of nuclear poly A(+) RNAs prepared from HeLa cells recovering from thermal stress (42°C for 2 h followed by recovery at 37°C for 1 h) in which YTHDC1 and HSATIII were sequentially knocked down with siRNA and ASO, respectively, before exposure to thermal stress. We also prepared nuclear polyA(+) RNAs from cells treated with control siRNA and/or control oligonucleotide (Fig 5A). As shown in Fig 5B, we first compared the effect of YTHDC1 KD and HSATIII KD on expression of HSATIII-target introns (blue dots) in whole introns annotated in our RNA-seq. We found weak negative correlation between the effect of YTHDC1 KD in HSATIII KD cells and HSATIII KD on HSATIII-target introns ($r = -0.29$) but not on whole introns ($r = -0.1$), probably because of the presence of numerous unrelated introns (Fig 5B). Namely most of the introns down-regulated upon HSATIII KD were up-regulated upon YTHDC1 KD (Fig 5B, blue dots). It was noteworthy that most of the exceptionally up-regulated introns by HSATIII KD were down-regulated by YTHDC1 KD (Fig 5B). These findings indicate that YTHDC1 generally produces effects on HSATIII-target introns that are opposite to those of HSATIII lncRNAs. Considering that HSATIII lncRNAs sequestrate YTHDC1 in nSBs, HSATIII lncRNAs may negatively regulate YTHDC1 splicing function.

The RNA-seq results identified that, in HSATIII KD cells, 1,791 and 1,083 introns were up- and down-regulated, respectively, upon YTHDC1 KD (|logFC ($\log_2$ fold change) |$\geqq$ 1 and $P < 0.01$) (Fig 5C). In contrast, 1,001 and 551 introns were up- and down-regulated, respectively, upon YTHDC1 KD in HSATIII-expressing cells (|logFC| $\geqq$ 1 and $P < 0.01$) (Fig 5C). This indicates that HSATIII lncRNAs broadly obscure the latent effect of YTHDC1 KD on intron retention, possibly by sequestration of YTHDC1 within nSBs. To address this issue more quantitatively, we calculated ΔlogFC (logFC in HSATIII KD cells – logFC in HSATIII-expressing cells) of YTHDC1-dependent introns. The 1,791 introns up-regulated upon YTHDC1 KD were classified into three groups: 1. 659 HSATIII-attenuated introns (ΔlogFC $\geqq$ 0.5), 2. 1,066 HSATIII-resistant introns (|ΔlogFC| < 0.5), and 3. 17 HSATIII-enhanced introns (ΔlogFC $\leqq -0.5$) (Fig 5D). Thus, HSATIII lncRNAs attenuated the effects of YTHDC1 KD on a subset of introns but minimally affected the remaining majority of introns (Fig 5D).

To understand the difference between the HSATIII-attenuated group (659 introns) and the other 1,083 introns among the YTHDC1 KD up-regulated introns, we investigated correlations between the ΔlogFC of total YTHDC1 KD up-regulated introns and various features, such as GC content and lengths of the introns and their adjacent exons. We found that the HSATIII attenuation effect on YTHDC1 dependency was negatively correlated with GC content of the introns (Fig 5E). The GC contents of 659 introns of the HSATIII-attenuated group (ΔlogFC $\geqq$ 0.5) were significantly lower than those of the other YTHDC1-dependent introns (ΔlogFC < 0.5) (Fig 5F). Among these 659 introns, 44 overlapped with 533 previously reported down-regulated introns upon HSATIII KD (Ninomiya *et al*, 2020) [Fig 5E (indicated by orange dots) and Appendix Table S2]. We, therefore, judged them to be promising target introns whose splicing is blocked by HSATIII-dependent sequestration of YTHDC1. The GC contents of the 44 YTHDC1-mediated HSATIII-target introns were extremely low (Fig 5F). HSATIII lncRNAs mainly promote intron retention but exceptionally suppress retention of a small number of introns (Ninomiya *et al*, 2020). We also performed the same analyses for introns down-regulated upon YTHDC1 KD and found the effect of YTHDC1 KD on 317 introns was attenuated by HSATIII lncRNAs (Figs 5D and EV3B). The GC content of the HSATIII-attenuated group was also significantly lower than that of the other introns, although its average value [47.5% (mean), 47% (median)] (Fig EV3C) was almost comparable to that of whole introns (Fig 5F). Two of seventeen introns previously reported to be down-regulated by HSATIII lncRNAs overlapped with 317 introns in

Figure 5. Two distinct mechanisms of nSB-dependent splicing control.

A Outline of RNA-seq-based screening for the introns regulated by HSATIII-dependent sequestration of YTHDC1.

B Scatter plot of LogFC of whole annotated introns (gray) and previously reported HSATIII-target introns (blue) upon sequential KD with HSATIII ASO and YTHDC1 siRNA (X-axis) and with HSATIII ASO and control siRNA (Y-axis, data from Ninomiya *et al*, 2020). Among 550 previously reported HSATIII-target introns, 47,374 whole introns and 461 annotated introns (|logFC| $\geqq$ 1, $P < 0.01$) were applied to the analysis. Pearson's correlation (r) is indicated above.

C Venn diagrams show the numbers of up- and down-regulated introns upon YTHDC1 KD (|logFC| $\geqq$ 1, $P < 0.01$) in HSATIII-expressing cells (magenta) and/or HSATIII-depleted cells (cyan).

D The number of introns classified by ΔlogFC of YTHDC1KD between HSATIII-expressing cells (control) and HSATIII KD cells (logFC upon YTHDC1 KD (HSATIII KD)-logFC upon YTHDC1 KD (Control)). Introns not applicable in any samples (not applicable) were omitted from the following analyses.

E Scatter plot of YTHDC1 KD up-regulated introns (logFC $\geqq$ 1, $P < 0.01$). The X- and Y-axes show the GC contents and ΔLogFC (HSATIII KD-control) of each intron, respectively. Magenta lines indicate |ΔLogFC| = 0.5. Analysis was applied to 1,742 introns (49 introns not applicable to the analysis were excluded from 1,791 introns). 659 introns (ΔLogFC $\geqq$ 0.5) were plotted above the upper magenta line.

F Boxplot of GC contents of three groups of introns up-regulated upon YTHDC1 KD [1,105 introns (ΔlogFC < 0.5 in D), 659 HSATIII-sensitive introns (ΔlogFC $\geqq$ 0.5 in D), and 44 YTHDC1-mediated HSATIII-target introns]. The GC content of 54,222 whole annotated introns is shown as a reference. The mean is indicated with X. The first and third quartiles are the ends of the box, the median is indicated with a vertical line in the box, and the minimum and maximum except for the outliers are the ends of the whiskers. The outliers are indicated with open circles. *P*-values (Kruskal–Wallis test, followed by Dunn's multiple comparison test) are shown above.

G Outline of RNA-seq in control and SRSF9 KD cells.

H Scatter plot of LogFC of whole introns (gray) and HSATIII-target introns (blue) upon SRSF9 KD (X-axis) and HSATIII KD (Y-axis). 51,469 and 548 introns are plotted as whole introns and previously reported HSATIII-target introns, respectively. Pearson's correlation (r) is indicated above.

I Venn diagram of introns down-regulated upon HSATIII KD (logFC $\leqq -1$, $P < 0.01$) (data from Ninomiya *et al*, 2020) and SRSF9 KD (logFC $\leqq -1$, $P < 0.01$), and HSATIII-sensitive YTHDC1-mediated introns (see Fig 5D and E).

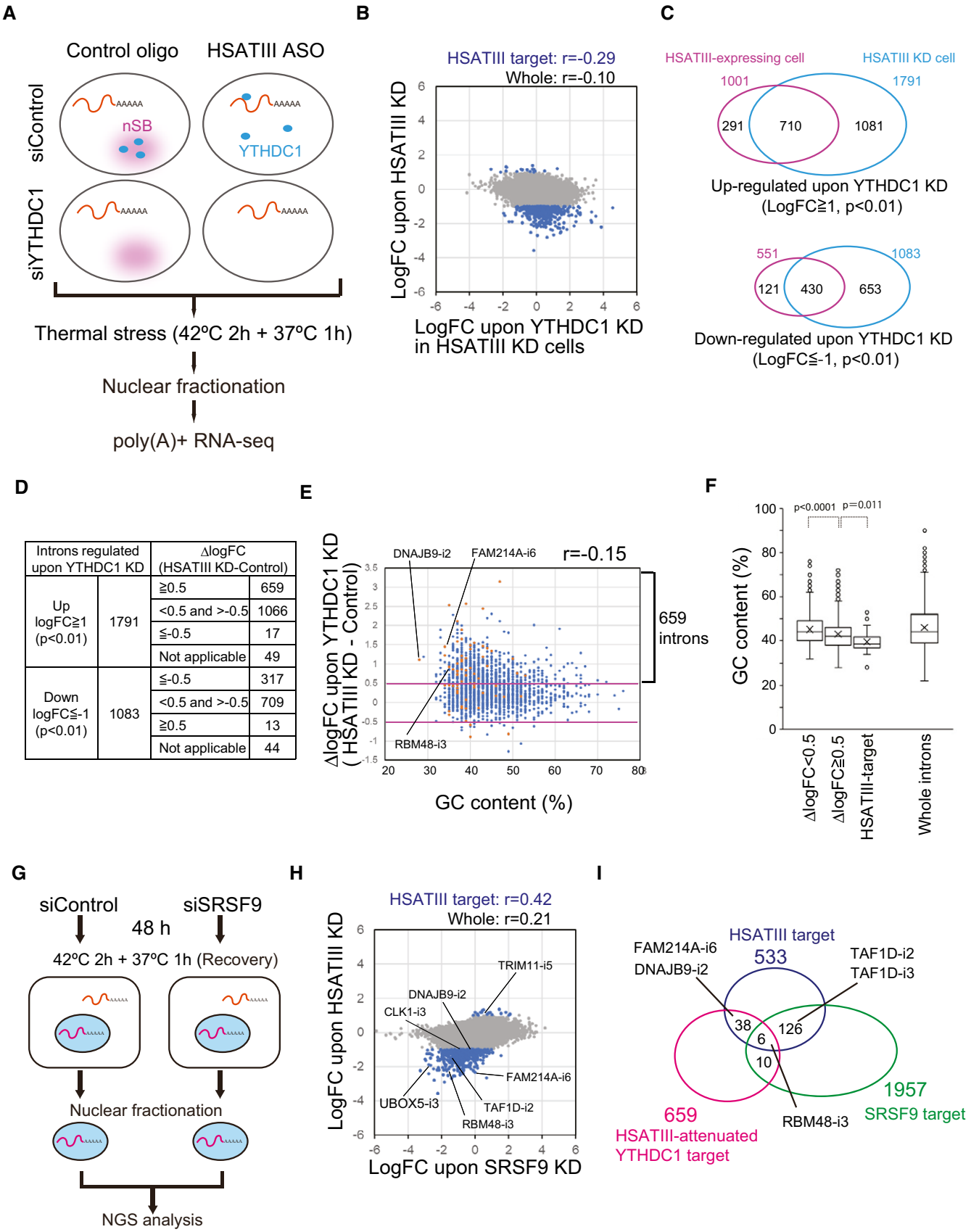

Introns regulated upon YTHDC1 KD		ΔlogFC (HSATIII KD-Control)	
Up logFC≧1 (p<0.01)	1791	≧0.5	659
		<0.5 and >-0.5	1066
		≦-0.5	17
		Not applicable	49
Down logFC≦-1 (p<0.01)	1083	≦-0.5	317
		<0.5 and >-0.5	709
		≧0.5	13
		Not applicable	44

Figure 5.

the HSATIII-attenuated group (Appendix Table S2). Taking these findings together, we argue that retention of HSATIII-target introns is regulated by two distinct pathways, SRSF9 phosphorylation and YTHDC1 sequestration, whose relationship we analyzed further (Figs 5G–I and EV3D–H) as described below.

YTHDC1 promotes splicing through m^{6}A methylation of nSB target pre-mRNAs

To experimentally validate the mechanism suggested above, we selected *FAM214A* intron 6 as a model. Consistent with our previous data (Ninomiya *et al*, 2020), RT–qPCR confirmed that the retention of *FAM214A* intron 6 was promoted after stress removal only in the presence of HSATIII (Fig 6A left). Consequently, promotion of intron retention down-regulated the production of the spliced *FAM214A* mRNA in control cells. In contrast, production of the spliced mRNA was up-regulated in HSATIII KD cells even after stress removal because of intron retention failure (Fig 6A right). We next asked if the failure of intron retention in HSATIII KD cells was prevented by YTHDC1 KD. To accurately quantify splicing efficiency during the stress recovery period, we prepared nascent RNAs labeled with 5-ethynyl uridine (5-EU), which are transcribed within 1 h after stress removal (Fig 6B). RT–qPCR using the nascent RNAs revealed that HSATIII KD promoted the splicing of *FAM214A* intron 6 (compare bars 1 and 3 in Fig 6C); however, the effect was prevented by YTHDC1 KD (compare bars 3 and 4 in Fig 6C). The splicing of *DNAJB9* intron 2, another YTHDC1-mediated HSATIII-target intron, was also promoted upon HSATIII KD and significantly prevented by YTHDC1 KD (Fig 6C). However, the effect is partial probably because this intron is also moderately regulated by the SRSF9-mediated mechanism (Ninomiya *et al*, 2020) (Fig 5H). We also confirmed that SRSF9-dependent splicing of *TAF1D* or *CLK1* was not affected by YTHDC1 KD even though HSATIII KD markedly promoted the splicing of these introns. This indicates that YTHDC1 does not affect splicing of *TAF1D* and *CLK1* introns regulated by SRSF9 (Fig 6F).

In addition, the splicing of *FAM214A* intron 6 was also suppressed by YTHDC1 KD under normal temperature conditions (Fig 6D). These data indicate that YTHDC1 promotes splicing of *FAM214A* intron 6 under normal conditions and that YTHDC1 released from nSBs by HSATIII KD promotes splicing under stress recovery conditions. WTAP KD also suppressed the splicing of *FAM214A* intron 6 (Fig 6D), raising the possibility that YTHDC1 regulates splicing of the specific intron through m^{6}A modification of the pre-mRNA. We performed m^{6}A-RIP-seq of control and HSATIII KD cells (Fig EV4A) and the m^{6}A peaks were visualized with our previous data of nuclear polyA(+) RNA-seq in the presence and absence of HSATIII (Ninomiya *et al*, 2020) (Figs 6E and EV4B). A single major m^{6}A peak was detected in *FAM214A* exon 6 (marked by an arrow in Fig 6E lower panel), adjacent to HSATIII-target intron 6 (underlined in Fig 6E upper panel). In control cells, this m^{6}A peak was markedly lower in stressed cells (42°C 2 h + 37°C 1 h, control) compared with that in unstressed cells (37°C, Control). However, in HSATIII KD cells, the m^{6}A peak was mostly unchanged, even after thermal stress (42°C 2 h + 37°C 1 h, HSATIII KD) (Fig 6E). m^{6}A-RIP followed by RT–qPCR using primers within *FAM214A* exon 6 (Fig 6C) confirmed that HSATIII lncRNAs suppressed m^{6}A modification of *FAM214A* (pre-)mRNAs (Fig 6F) without affecting total levels of *FAM214A* (pre-)mRNAs (Fig EV4C). Additionally, we also found that retention of *TRIM11* intron 5 was exceptionally up-regulated upon HSATIII KD (Ninomiya *et al*, 2020). This intron was down-regulated by HSATIII-dependent sequestration of YTHDC1 (Fig EV3B, Appendix Table S2), and the m^{6}A peaks located at the boundary of intron 5 and downstream exon 6 were increased upon HSATIII KD (Fig EV4C).

Taken together, our results indicate that nSBs promote intron retention of *FAM214A* intron 6 through two related mechanisms: first, suppression of m^{6}A modification and concomitant suppression of YTHDC1 binding in exon 6 and second, sequestration of YTHDC1 onto m^{6}A-modified HSATIII in nSBs from nucleoplasm, which may further suppress YTHDC binding in exon 6. Both mechanisms reduce YTHDC1 binding to the adjacent exon 6 and would negatively regulate splicing or promote retention of intron 6. The first mechanism of suppression of m^{6}A modification in exon 6 is likely to be caused by sequestration of the m^{6}A writer complex in nSBs. This is supported by our result showing that WTAP KD down-regulated the splicing of intron 6 (Fig 6D). The sequestered m^{6}A writer complex would substantially methylate HSATIII to sequester YTHDC1 in nSBs.

Two distinct nSB mechanisms for splicing control

We next addressed the relationship between two distinct pathways, SRSF9 phosphorylation and YTHDC1 sequestration, for the retention of HSATIII-target introns. We performed nuclear polyA(+) RNA-seq after SRSF9 KD to classify the HSATIII-target introns into those regulated by SRSF9 phosphorylation or YTHDC1 sequestration (Fig 5G). SRSF9 KD affected accumulation and/or splicing of numerous mRNAs probably through multiple direct or indirect pathways (Fig EV3D). We compared the effects of SRSF9 KD and HSATIII KD on previously reported HSATIII-target introns and whole detected introns and found positive correlation between them [HSATIII-target introns (r = 0.42), whole introns (r = 0.21)] (Fig 5H). The exceptionally up-regulated introns by HSATIII KD also tend to be up-regulated upon SRSF9 KD (Fig 5H). Taken together, our data indicated that SRSF9 and YTHDC1 mediate HSATIII-dependent regulation of intron retention; however, their effects were most likely opposite. If these proteins mediate regulation of HSATIII-dependent splicing via a common pathway in mutually opposite directions, their effects on individual HSATIII-target introns would be negatively correlated. However, their effects on HSATIII-target introns as well as on whole detected introns were not correlated (Fig EV3E), indicating that these proteins modulate HSATIII-target introns via independent mechanisms.

We identified 132 intron retention events that were promoted by both HSATIII and SRSF9 (Fig 5I, Appendix Table S3). For example, *TAF1D* introns 2 and 3 were regulated by both HSATIII and SRSF9, which is consistent with our previous experiments (Ninomiya *et al*, 2020), but not by YTHDC1 (Fig 6C). In contrast, *FAM214A* intron 6, which is regulated by HSATIII-dependent YTHDC1 sequestration (Fig 5E), was hardly affected by SRSF9 KD (Fig 5H). Six introns, including *RBM48* intron 3, were classified into a group regulated by both SRSF9 sequestration and YTHDC1 sequestration (Fig 5I, Appendix Tables S2 and S3), indicating that splicing of these introns is cooperatively suppressed by both the SRSF9- and YTHDC1-mediated mechanisms within nSBs. In other cases, the effects of

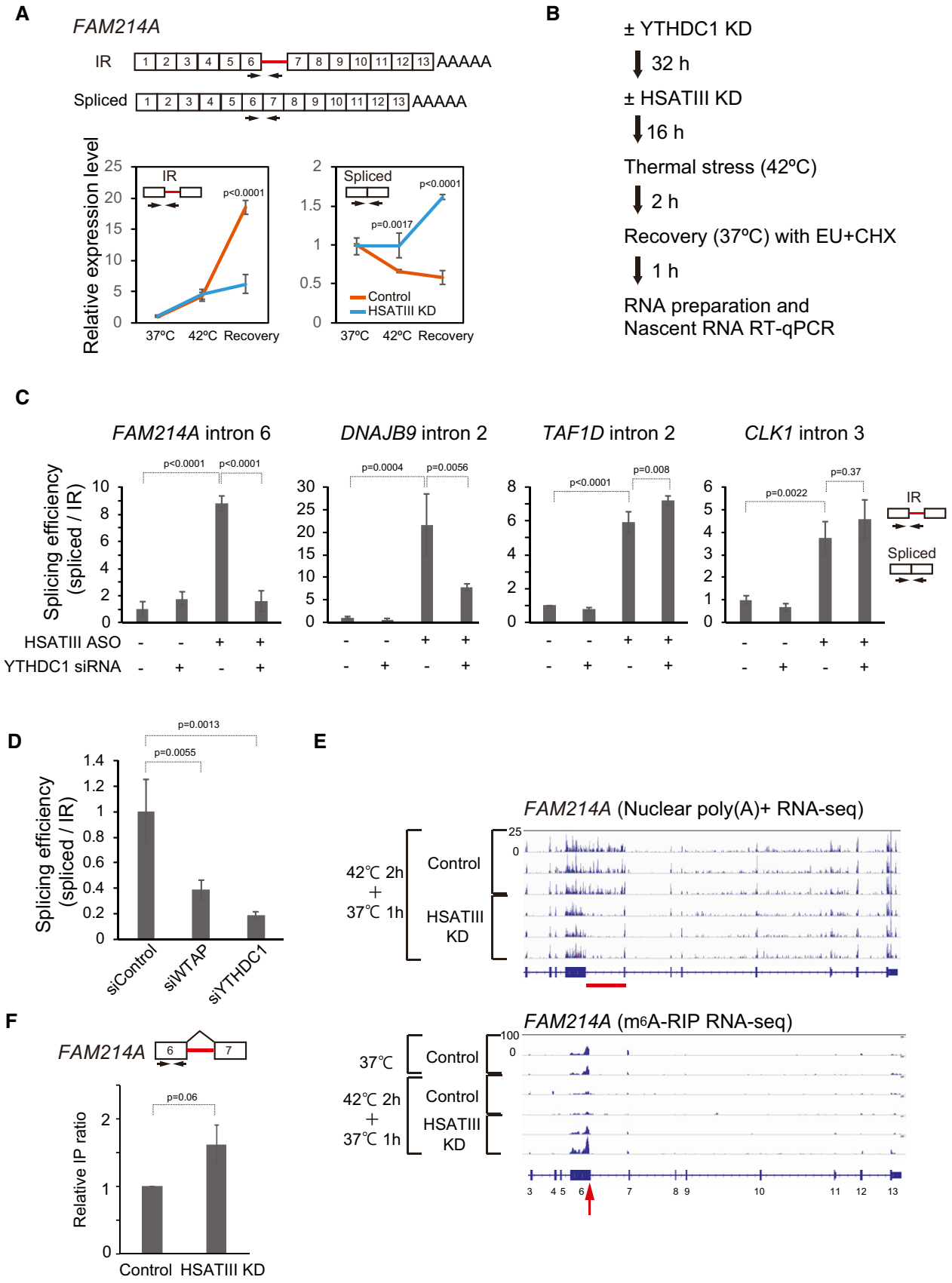

Figure 6.

Figure 6. m^{6}A factor sequestration-mediated splicing regulation.

A RT–qPCR analysis of *FAM214A* mRNA splicing. Intron-retaining isoforms (IR) of the *FAM214A* pre-mRNA are illustrated above. The retained intron is indicated by a red line. Arrows indicate the positions of the PCR primers used. The graphs show the relative amounts of the IR (left) and spliced (right) forms in control and HSATIII KD cells under three conditions: 37°C, 42°C for 2 h, and 42°C for 2 h followed by recovery at 37°C for 1 h (recovery). Expression levels were calculated as the ratio of each RNA to *GAPDH* mRNA and were normalized to the levels in control cells under normal conditions (37°C). Data are shown as the mean ± SD (n = 3); P-values ($P < 0.05$, Sidak's multiple comparisons tests) are shown above.

B Outline of RT–qPCR analysis of nascent RNAs upon HSATIII and YTHDC1 KD.

C RT–qPCR validation of splicing of nascent RNAs. Splicing efficiency of nascent RNAs was quantified as the ratio of the spliced form to the intron retaining isoform (IR) form and normalized to the control. Control siRNA and HSATIII control oligonucleotide are indicated with (−). Data are shown as the mean ± SD (n = 3); P-values (Tukey's multiple comparison test) are shown above.

D m^{6}A-dependent splicing of *FAM214A* intron 6. HeLa cells were transfected with control (siControl), WTAP (siWTAP), or YTHDC1 (siYTHDC1) siRNA and cultured for 48 h. PCR primers are the same as in A. Splicing efficiency was calculated using the method described in C and normalized to the control (siControl). Data are shown as the mean ± SD (n = 3); P-values (Dunnett's multiple comparison test) are shown above.

E Read maps represent RNA-seq data of nuclear poly(A)+ RNAs (upper panel, biological triplicate) and m^{6}A-RIP RNAs (lower panel, biological duplicate) in control and HSATIII KD cells. The exon numbers of the *FAM214A* gene are indicated below. The retaining intron and the m^{6}A peak are marked by a red line and arrow, respectively. For the entire *FAM214A* region, see also Fig EV4B.

F RT–qPCR validation of m^{6}A-RIP of *FAM214A* mRNA. The positions of primers are indicated above. Relative pulldown efficiency of each experiment was calculated as the ratio of pulldown efficiency (pulldown/input) in HSATIII KD cells to that in control cells. Data are shown as the mean ± SD (n = 3); P-value (Welch's t-test) is shown above.

SRSF9 and HSATIII-mediated YTHDC1 sequestration seem to neutralize each other with regard to splicing regulation. For example, *UBOX5* intron 3 was down-regulated by SRSF9 KD (Fig 5H), but up-regulated by HSATIII-dependent sequestration of YTHDC1 (Fig EV3B), indicating the existence of introns whose splicing is regulated by HSATIII lncRNAs via both SRSF9- and YTHDC1-mediated mechanisms, although total splicing remained unchanged because of their neutralization effect. We also found that the negative correlation between the effects of YTHDC1 KD and HSATIII KD ($r = -0.29$, Fig 5B) became stronger ($r = -0.35$), when the 132 introns regulated by the SRSF9-dependent mechanism were excluded from whole HSATIII-target introns (Fig EV3F).

The GC content of the 44 YTHDC1-mediated HSATIII-target introns was similar to that of whole HSATIII-target introns (Fig EV3G), which is in contrast to the GC content of 132 SRSF9-dependent HSATIII-target introns and was significantly higher than that of whole HSATIII-target introns (Fig EV3G). We also detected a higher frequency of GRACH motifs, which the m^{6}A writer complex recognizes, in the adjacent upstream and downstream exons of HSATIII-regulated YTHDC1-dependent introns (Appendix Table S4). As we previously reported, the sizes of upstream and downstream exons of HSATIII-target introns tend to be larger than the average intron size (Ninomiya *et al*, 2020). We, therefore, analyzed the sizes of adjacent exons of SRSF9- and YTHDC1-mediated HSATIII-target introns, except for the first and last exons, because they generally tend to be longer. The upstream exons of YTHDC1-dependent intron subset were particularly longer compared with whole HSATIII-target introns or SRSF9-dependent intron subset, whereas the downstream exons tend to be prominently shorter than those of the other groups (Fig EV3H). These results indicate that the distinct features of target introns and adjacent upstream exons are involved in recognition by the two distinct mechanisms. In addition, upstream and downstream exons of HSATIII-regulated YTHDC1-dependent introns tend to be longer than those of the HSATIII-unregulated group (Fig EV3H).

The RNA-seq analyses above indicated that SRSF9- and YTHDC1-mediated mechanisms work independently in regulating splicing of HSATIII-target introns. To experimentally validate independence of the two pathways, we performed splicing reporter assays with retention of *DNAJB9* intron 2 as a model system, which is concurrently regulated via both the SRSF9- and YTHDC1-mediated mechanisms [Fig 6C and (Ninomiya *et al*, 2020)]. The relatively short length of *DNAJB9* intron 2 and the adjacent exons makes then suitable for a splicing reporter minigene. The m^{6}A-RIP RNA-seq data show that the major m^{6}A peak was detected on the adjacent exon 3 of the *DNAJB9* (pre-)mRNA and was up-regulated upon HSATIII KD (Fig EV5A). Then, we constructed splicing reporters harboring two *DNAJB9* minigenes with exon 3 of different lengths (Fig EV5B). Splicing of the shorter reporter RNA (minigene#1) lacking the m^{6}A site was hardly affected by YTHDC1 KD, whereas that of the longer minigene possessing the m^{6}A site (minigene#2) was substantially suppressed (Fig EV5B). This result supports the splicing of this intron being dependent on YTHDC1 binding to the m^{6}A peak on exon 3. In contrast, SRSF9 KD moderately but equally up-regulated splicing of both of the above reporter RNAs (Fig EV5B). We also compared the effects of wild-type SRSF9 (SRSF9 WT) and its phosphorylation-deficient mutant (SRSF9-mut) (Ninomiya *et al*, 2020) on splicing of the *DNAJB9* reporter (minigene #2). Splicing of *DNAJB9* intron 2 was more efficient in the SRSF9-mut-expressing cells compared with the SRSF9 WT-expressing cells even at normal temperature (Fig EV5C), indicating that deficient phosphorylation of SRSF9 prevented intron retention and allowed splicing of *DNAJB9* intron 2. These data indicate that production of the spliced form of *DNAJB9* mRNA is blocked cooperatively by both m^{6}A-mediated YTHDC1 sequestration and SRSF9-mediated mechanisms. Collectively, these results support the model that the m^{6}A- and SRSF9-mediated mechanisms within nSBs control splicing of distinct but not mutually exclusive subsets of HSATIII-target introns.

The m^{6}A methylated and the unmethylated GGAAU repeat sequences of HSATIII can be a platform for dual-splicing control mechanisms through two distinct RNP complexes

HSATIII lncRNAs consist mostly of GGAAU repeats; therefore, our results above provoke a simple question: Is the GGAAU repeat sufficient to form a common platform for the dual-splicing control mechanisms, SRSF9 phosphorylation, and sequestration of m^{6}A-related factors. To address this point, we performed *in vitro* pulldown

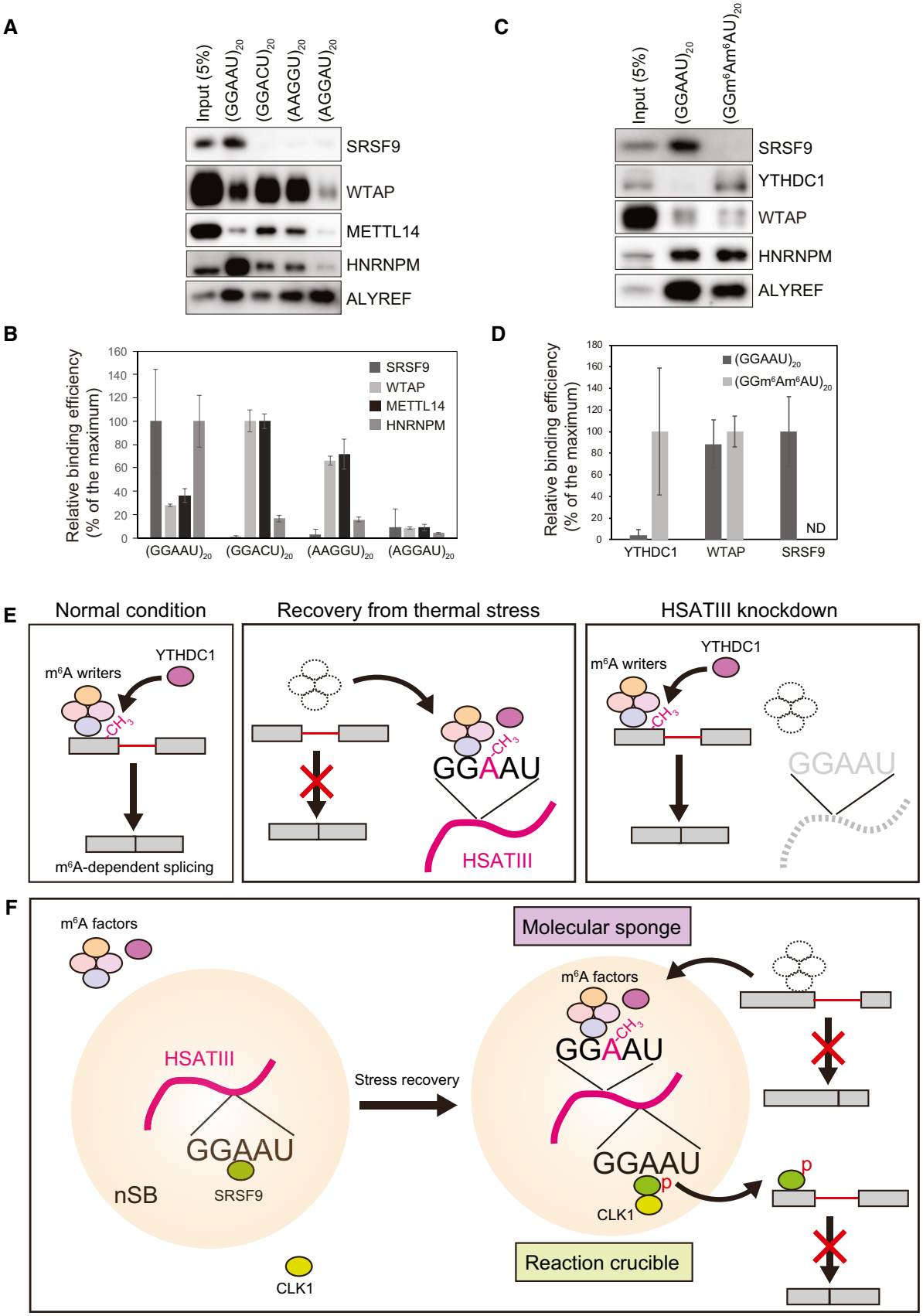

Figure 7.

Figure 7. The partially m^{6}A-methylated GGAAU repeat sequence is a common platform for the dual mechanisms of splicing control.

A *In vitro* pulldown assay of RNP complexes with various repeat RNAs. *In vitro* RNA pulldown was performed using biotinylated (GGAAU)×20 and other three repeat RNAs incubated in HeLa nuclear extract. The co-precipitated proteins were detected by Western blotting using specific antibodies. ALYREF, a non-specific RNA-binding protein, was used as a control.

B Quantification of data in A. Relative co-precipitation efficiency of each protein was normalized by the maximum value. Data are shown as the mean ± SD (n = 3).

C *In vitro* pulldown assay with methylated GGAAU repeat RNA. *In vitro* RNA pulldown assay was performed using biotinylated GGAAU and GGm^{6}Am^{6}AU repeat RNAs as in A.

D Quantification of data in C. Relative co-precipitation efficiency of each protein was normalized by the maximum value. Data are shown as the mean ± SD (n = 3).

E Model of nSB function in splicing control through protein sequestration. Under normal conditions, the m^{6}A writer complex methylates specific sites of the target mRNA, which then recruits YTHDC1 to promote splicing (left). During recovery from thermal stress, HSATIII lncRNAs sequester the m^{6}A writer complex, which diminishes m^{6}A methylation and YTHDC1 binding to repress splicing of the target mRNA. YTHDC1 is also sequestered by the methylated HSATIII lncRNA (middle). In HSATIII KD cells, the target mRNA can be methylated and recruits YTHDC1 to promote splicing even during thermal stress recovery (right).

F Significance of the partially m^{6}A-methylated GGAAU repeat sequence of HSATIII lncRNA in the dual mechanisms of splicing control in nSBs. HSATIII lncRNAs act as a molecular sponge for sequestration of m^{6}A-related proteins via the m^{6}A-methylated region and as a reaction crucible for CLK1-dependent rephosphorylation of SRSFs via the unmethylated region. Both mechanisms repress splicing of respective target mRNAs during thermal stress recovery.

Source data are available online for this figure.

assays using biotinylated *in vitro* transcribed RNAs with sequences $(GGAAU)_{20}$, $(GGACU)_{20}$, $(AAGGU)_{20}$, and $(AGGAU)_{20}$ in HeLa cell nuclear extract. SRSF9, WTAP, and METTL14 were co-precipitated with $(GGAAU)_{20}$ RNA. SRSF9 specifically bound $(GGAAU)_{20}$ but not the other three repeats (Fig 7A and B). $(GGACU)_{20}$, which matches the consensus sequence (UGGACU) for binding the m^{6}A writer complex (Schibler *et al*, 1977; Harper, Miceli *et al*, 1990), captured WTAP and METTL14 most efficiently but not SRSF9 (Fig 7A and B). $(AAGGU)_{20}$ also captured WTAP and METTL14 but not SRSF9. In contrast, $(AGGAU)_{20}$ hardly captured any of these proteins. It was noteworthy that WTAP and METTL14 showed almost identical sequence selectivity for binding (Fig 7B), indicating that WTAP and METTL14 interacted with RNAs as a complex. These results indicate that the GGAAU repeat can be a common scaffold for SRSF9 and WTAP/METTL14, even though the amounts of WTAP and METTL14 bound with GGAAU *in vitro* were 28 and 36%, respectively, relative to those bound to the GGACU consensus sequence. In addition, we confirmed that HNRNPM, a component of a distinct nSBs subclass, nSB-M (Aly, Ninomiya *et al*, 2019), was also efficiently co-precipitated with the GGAAU repeat RNA (Fig 7A and B). ALYREF was co-precipitated with all repeat RNAs, which are consistent with ALYREF promiscuously binding RNAs (Viphakone, Sudbery *et al*, 2019). Next, we examined *in vitro* transcribed $(GGm^6Am^6AU)_{20}$ RNA and found that YTHDC1 co-precipitated well with $(GGm^6Am^6AU)_{20}$ but poorly with unmethylated $(GGAAU)_{20}$ (Fig 7C and D). In contrast, SRSF9 was not co-precipitated with $(GGm^6Am^6AU)_{20}$, indicating that SRSF9 selectively interacts with the unmethylated regions of HSATIII lncRNAs (Fig 7C and D). We suggest that GGAAU repeat RNA with partial m^{6}A modification allows a common platform for the formation of two distinct RNP complexes, with SRSF9 or WTAP/METTL14, for at least two functionally distinct regulatory mechanisms in nSBs.

Discussion

We recently reported that nSBs function as "reaction crucibles" under thermal stress conditions, in which HSATIII lncRNAs concentrate dephosphorylated SRSF1 and SRSF9 as substrates, and that after stress removal, the enzyme CLK1 is recruited to rapidly rephosphorylate the pre-captured SRSFs (Ninomiya *et al*, 2020). In this study, we discovered that HSATIII lncRNAs are m^{6}A-methylated in the GGAAU repeat and sequester YTHDC1 within nSBs from the nucleoplasm, especially during thermal stress recovery, which results in repression of m^{6}A-dependent splicing of specific pre-mRNAs (Fig 7E). Thus, nSBs play dual functions as "molecular sponges" for YTHDC1 sequestration as well as "reaction crucibles" for SRSF phosphorylation (Fig 7F). Interestingly, both mechanisms contribute to a common cellular function: transient repression of pre-mRNA splicing during thermal stress recovery. These two mechanisms work independently in distinct target introns recognizing different features: lower GC content and longer upstream exon for the YTHDC1 pathway, and relatively longer downstream exon for the SRSF9 pathway. However, at least a subset of HSATIII-target introns, such as *RBM48* intron 3, is regulated cooperatively by both mechanisms.

As we recently reported (Ninomiya *et al*, 2020), the patterns of HSATIII-target intron changes are classified into two distinct classes; class 1 introns (e.g., *CLK1* intron 3 and *TAF1D* introns 2/3) are retained at substantial levels under normal conditions, but are excised during thermal stress and re-accumulated during stress recovery, and class 2 introns (e.g., *DNAJB9* intron 2 and *FAM214A* intron 6), which are mostly excised under normal and thermal stress conditions but specifically retained during stress recovery. The distinct features of the temperature-dependent splicing of the two intron classes can be explained by the presence of two distinct regulatory mechanisms involving "reaction crucibles" and "molecular sponges". More specifically, phosphorylated SRSF9, which is active in suppressing target intron splicing in normal conditions, is dephosphorylated upon thermal stress and rapidly re-phosphorylated to return to its active form in nSBs (Ninomiya *et al*, 2020). In contrast, YTHDC1, which promotes m^{6}A-dependent splicing in normal conditions, is sequestered in nSBs during stress recovery, thereby suppressing the splicing of target introns (Fig 7E). Thus, both mechanisms enable the control of gene expression through intron retention upon acute temperature change. Consistently, genes associated with response to heat stress and unfolded proteins, whose expression is transiently required during thermal stress conditions, are enriched among the genes regulated via the SRSF9 pathway (Appendix Table S5).

Our RNA-MS analysis of purified HSATIII lncRNAs showed that the GGAAU repeat is m^{6}A-modified. GGm^{6}AAU has a mismatch to GRm^{6}ACH, the well-established consensus motif for the METTL3/14-containing m^{6}A writer complex; therefore, it is uncertain whether

the HSATIII repeat sequence can be a potent substrate because the cytosine next to the A to be modified is widely believed to be essential for substrate recognition (Schibler *et al*, 1977). However, as shown in Fig 7A and B, WTAP and METTL14 can substantially interact with GGAAU repeat RNA *in vitro*, even though the binding affinity is only ~30% of that with the consensus GGACU repeat. Considering that HSATIII lncRNAs are highly abundant in the nuclei of thermally stressed cells and each RNA contains many copies of the GGAAU repeat, the weaker affinity of the m^6A writer complex for GGAAU might be enough to competitively sequester the m^6A writer complex from m^6A modification of other nucleoplasmic RNAs. It is also possible that cofactor(s) within nSBs modify the recognition motif of the writer complex *in vivo* to methylate the GGAAU repeat sequence. HSATIII lncRNAs sequestrate m^6A factors by acting as substrates for methylation. This means that HSATIII selectively sequestrates "functional" m^6A writer complex, which can bind the substrate RNAs. Therefore, the actual impact of HSATIII-dependent sequestration on other nuclear RNAs must be greater than what we estimated by immunostaining, which visualizes both functional and non-functional proteins (Fig 4). Interestingly, our RNA-seq analyses revealed that HSATIII lncRNA-dependent sequestration of m^6A factors can prevent YTHDC1-dependent splicing of introns with low rather than high GC content. This raised the possibility that m^6A modification and YTHDC1-dependent splicing of lower GC content introns are more sensitive to sequestration of m^6A factors, which might be influenced by the factors associated with the surrounding sequences. This selectivity also raises another possibility that the m^6A writer complex is modified within nSBs so as not to methylate pre-mRNAs with low GC content introns or that the pre-mRNAs are processed in close proximity to nSBs, where the sequestration is more effective. Alternatively, HSATIII may selectively affect introns whose adjacent upstream exons possess more frequent GRACH motifs (Appendix Table S4) through the effect of combined sequestration of m^6A writer complexes and YTHDC1.

Our HSATIII-ChIRP-MS analysis identified the major components of the METTL3/14-containing writer complex as HSATIII lncRNA-interacting proteins except for the catalytic subunits, METTL3 and METTL14 (Fig 1A, Dataset EV1). Nevertheless, METTL3/14 KD inhibited m^6A accumulation and YTHDC1 recruitment into nSBs (Figs 1K and L, and EV1G and H), indicating that the catalytic subunits transiently interact with HSATIII lncRNAs and dissociate from the m^6A-modified RNAs. m^6A modification is also involved in the control of other RNA metabolic processes, such as transcription, RNA export, RNA decay, and translation. Our ChIRP-MS analysis identified other m^6A reader proteins, including RBMX (HNRNPG) and HNRNPA2/B1 as nSB components, which are involved in m^6A-dependent control of miRNA maturation and co-transcriptional splicing (Bi, Liu *et al*, 2019; Zhou *et al*, 2019). Thus, it is also possible that HSATIII-dependent sequestration of m^6A writer and reader proteins may modify other processes of RNA metabolism as well as splicing.

Our *in vitro* binding experiments (Fig 7A and B) indicate that GGAAU repeat RNAs allow dual mechanisms for transient splicing control during thermal stress recovery. In particular, the data in Fig 7C and D indicate that m^6A modification contributes to the assembly of two distinct RNP complexes containing either SRSF9 or YTHDC1 on an RNA with the GGAAU repeat. This suggests that the efficiency of m^6A modification determines the ratio of the two RNP complexes formed on HSATIII lncRNAs, which may impact the transcriptome during stress recovery.

Our findings regarding nSB functions provoke a fundamental question: Why have primates obtained such dual splicing control mechanisms that work specifically during stress recovery? Recent studies have reported that CLK1-dependent phosphorylation of SRSFs and intron retention as well as m^6A modification are regulated synchronously with respect to the circadian clock and cell cycle (Fustin, Doi *et al*, 2013; Dominguez, Tsai *et al*, 2016; Preußner, Goldammer *et al*, 2017). An intriguing possibility is that HSATIII lncRNA-based nSBs adjust rhythmic expression of genes after stress removal by transiently repressing splicing of multiple introns. From another point of view, genes associated with prostate gland development and prostate cancer progression (Appendix Table S5) are identified as YTHDC1 pathway-dependent HSATIII-target genes. For example, androgen receptor (AR) is a cofactor of HSP and a major player in PC progression (Hessenkemper & Baniahmad, 2013). AR pathway-related genes were also enriched in SRSF9-mediated HSATIII-target genes (Appendix Table S5). HSATIII lncRNA may reduce the risk of anomalous prostate gland development or prostate cancer progression by suppressing these genes after thermal stress. It would be intriguing to investigate the specific tissues in primates that are sensitive to thermal stress, such as the prostate gland, where HSATIII-dependent regulatory mechanisms may effectively act to normalize complicated physiological pathways during stress recovery.

Materials and Methods

Cell culture and knockdown

HeLa cell culture, knockdown, and thermal stress induction were performed as previously reported (Ninomiya, Adachi *et al*, 2020). Oligonucleotides and siRNAs for knockdown are listed in Appendix Table S6.

ChIRP-MS

ChIRP-MS was performed with HeLa cells at various thermal stress time points as previously reported (Ninomiya *et al*, 2020). Briefly, cultured cells at 80–90% confluency were immediately crosslinked in 10 ml 1% paraformaldehyde (PFA)/PBS per 10-cm dish for 15 min at room temperature and collected in microtubes by microcentrifugation. The collected cells were resuspended in 350 µl lysis buffer [50 mM Tris-Cl pH 7.0, 10 mM EDTA, 1% SDS, 1 mM PMSF, cOmplete™ Protease Inhibitor Cocktail (Sigma), and RNAse inhibitor (Thermo Fisher Scientific)] and disrupted using a Bioruptor (Cosmo Bio) (15 s ON, 45 s OFF, 118 cycles). Subsequently, the insoluble fraction was removed by microcentrifugation for 10 min at 15°C, and the supernatant was used for ChIRP. Two volumes of hybridization buffer [750 mM NaCl, 1% SDS, 50 mM Tris-Cl pH 7.0, 1 mM EDTA, 15% (v/v) formamide, 1 mM PMSF, cOmplete™ Protease Inhibitor Cocktail (Sigma), and RNAse inhibitor] and the biotinylated HSATIII antisense oligonucleotide (ASO) were added. The mixture was incubated at 37°C for 4 h, and the biotinylated HSATIII ASO was captured with Dynabeads MyOne Streptavidin C1 (Thermo Fisher Scientific). The beads were then washed five times for 5 min at 37°C with 0.8 ml wash buffer (2× SSC and 0.5% SDS).

The bound proteins were eluted and reverse-crosslinked by boiling in 100 mM Tris–HCl (pH 8.0) with 2% SDS (95°C for 30 min). The eluted samples were subjected to mass spectrometry as previously reported (Ninomiya *et al*, 2020).

RNA-MS

HSATIII RNA fragments were isolated by ChIRP, purified as previously reported (Ninomiya *et al*, 2020), treated with RQ1 RNase-free DNase (Promega), and precipitated using biotinylated HSATIII ASO and streptavidin magnetic beads. Precipitated RNAs and RNAs in the supernatant were purified as HSATIII RNAs and nSB-associated non-HSATIII RNAs, respectively, using TRI Reagent or TRI Reagent LS (Molecular Research Center, Inc.). For RNA fragment analysis, the purified HSATIII lncRNAs (approximately 100 ng) were digested with RNase T1 (Thermo Fisher Scientific) in 20 mM NH_4OAc (pH 5.3) at 37°C for 30 min and then mixed with the same volume of 0.1 M trimethylamine acetate (pH 7.0). The digests were analyzed by a splitless nanoflow high-performance LC system (DiNa, Techno Alpha) using a trap column and a capillary column (HiQ Sil C18W-3, 0.1 × 100 mm, Techno Alpha). The molecular mass of each fragment was calculated by deconvolution of the multivalent negative ions in the mass spectra. Nucleoside analysis was performed as described previously (Akichika, Hirano *et al*, 2019). The frequency of m^6A was quantified using the peak intensity ratio of m^6AAUG and m^6Am^6AUG to total AAUG nucleotides. For nucleoside analysis, the purified HSATIII lncRNAs were digested into nucleosides with 0.1 units of nuclease P1 (Fujifilm Wako Pure Chemical Corporation), 0.2 units PDaseI (Worthington Biochemical Corporation), and 0.1 units of bacterial alkaline phosphatase(Takara) and subjected to LC/MS analysis using a Q Exactive Hybrid Quadrupole-Orbitrap Mass Spectrometer (Thermo Fisher Scientific) equipped with a Dionex UltiMate 3000 LC System (Thermo Fisher Scientific) and ZIC-cHILIC Column (3 μm, 2.1 × 150 mm, Merck), as described previously (Sakaguchi, Miyauchi *et al*, 2015).

Fluorescent in situ hybridization (FISH) and immunofluorescence (IF)

FISH and IF were performed as previously reported (Ninomiya *et al*, 2020) with minor modifications. For m^6A immunostaining, cells were fixed in 4% paraformaldehyde/PBS (pH 7.4) overnight at 4°C, treated with 0.2 N HCl for 20 min at RT, and washed with RNase-free water. Then, the cells were treated with 1 μg/ml Proteinase K in protease buffer [100 mM Tris–HCl (pH 8.0), 50 mM EDTA (pH 8.0)] for 10 min at 37°C, incubated in 0.2% glycine/PBS for 10 min at RT, washed with PBS, and fixed again in 4% paraformaldehyde/PBS (pH 7.4) for 20 min at RT, followed by hybridization steps as previously described (Ninomiya *et al*, 2020). Antibodies and probes used are listed in Appendix Table S6.

RT–qPCR and semi-quantitative RT–PCR

RT–qPCR, semi-quantitative RT–PCR, and nascent RNA RT–qPCR were performed as previously reported (Ninomiya *et al*, 2020). For nascent RNA preparation, 100 μg/ml cycloheximide (CHX) was added during EU-labeling to detect NMD (nonsense-mediated mRNA decay)-targeted RNAs. Primers used are listed in Appendix Table S7.

Western blotting

Western blotting was performed as previously reported (Ninomiya *et al*, 2020). Antibodies used are listed in Appendix Table S6.

RNA-seq

For SRSF9 knockdown, HeLa cells were transfected with control or SRSF9 siRNAs and cultured for 48 h. For double knockdown of HSATIII and YTHDC1, HeLa cells were transfected with control or YTHDC1 siRNA using Lipofectamine RNAi MAX reagent (Thermo fisher) and cultured for 36 h, then transfected with HSATIII antisense oligonucleotide (ASO) or control sense oligonucleotide (SO) by nucleofection using Cell Line Nucleofector Kit R (LONZA) and cultured for 18 h. After thermal stress induction (42°C 2 h followed by 37°C 1 h), nuclear fractionation and RNA preparation were performed as previously described (Ninomiya *et al*, 2020). Poly(A)+ RNA purification and library construction were performed using 200 ng of total nuclear RNAs and the Illumina TruSeq Stranded mRNA HT Sample Prep Kit. Subsequently, RNA-seq was performed using the Illumina Novaseq6000 system with the 50-bp pair end method.

Bioinformatics

Bioinformatic analysis of RNA-seq data was performed as previously reported (Ninomiya *et al*, 2020) with a few exceptions. For quality control of RNA-seq reads, low-quality and ambiguous bases were trimmed, and trimmed reads shorter than 30 bp were filtered out using cutadapt (version 2.0) (Martin, 2011) with the parameters: --cores=10 --nextseq-trim=30 --max-n 0 -m 30. After the quality control process, the remaining reads were mapped to the human reference genome (hg38) with GENCODE gene annotation (release 27) (Frankish, Diekhans *et al*, 2019) using STAR aligner (version 2.5.3a) (Dobin, Davis *et al*, 2013) with the parameters: --runThreadN 10 --outSAMtype BAM SortedByCoordinate --quantMode GeneCounts --twopassMode Basic. The expression analysis of exons/introns in representative transcripts [selected from GENCODE annotation using CGAT scripts (version 0.3.2) (Sims, Ilott *et al*, 2014)] was conducted as previously reported (Ninomiya *et al*, 2020). Briefly, the mapped reads were counted using featureCounts (subread-1.4.6) (Liao, Smyth *et al*, 2014) with following parameters: -p -s 2 -T 10 -t exon -g exon_id. Differential expression analysis was performed using DESeq2 (version 1.10.1) (Love, Huber *et al*, 2014) with default parameters. The RNA-seq data derived from YTHDC1 deficient and control samples (Xiao, Adhikari *et al*, 2016) were also analyzed using the aforementioned computational pipeline with two exceptions (cutadapt parameters: --cores=10 -q 30 --max-n 0 -m 75 and featureCounts parameters: -p -s 0 -T 10 -t exon -g exon_id). The consensus motif (GRACH) for m^6A modification in exon/intron sequences was counted by using regular expression of Perl script.

m^6A-RIP-seq

Total RNAs were prepared from control and HSATIII knockdown cells using TRI Reagent (Molecular Research Center, Inc.). The intact mRNAs were isolated using a Seq-Star poly(A) mRNA Isolation Kit (Arraystar) and chemically fragmented to approximately 100-nt fragments. m^6A-RIP was performed with an anti-N6-

methyladenosine (m^6A) antibody to enrich for m^6A-methylated mRNA fragments. The RNA-seq libraries for both the m^6A immunoprecipitated RNAs and the input RNAs were prepared with a KAPA Stranded mRNA-seq Kit. The barcoded libraries were denatured to single-stranded DNAs, captured on Illumina flow cells, amplified in situ as sequencing clusters, and sequenced for 300 cycles on the Illumina HiSeq 4000 system according to the manufacturer's instructions. Sequencer image analysis and base calling were performed using Solexa pipeline v1.8 (Off-Line Base Caller software, v1.8). Sequencing read quality was examined by FastQC software. The clean reads (that passed the Illumina quality filter and adapter trimmed by Trimmomatic) were aligned to the Ensembl reference genome using HISAT2 software (v2.1.0).

m^6A-RIP–qPCR

HeLa cells were transfected with HSATIII ASO (HSATIII KD) or sense oligonucleotide (SO) and cultured for 16 h and exposed to thermal stress (42°C 2 h followed by 37°C 1 h). During the recovery period, 100 μg/ml cycloheximide (CHX) was added to detect NMD-targeted RNAs. Total RNAs were prepared from control and HSATIII knockdown cells using TRI Reagent or TRI Reagent LS (Molecular Research Center, Inc.) and subjected to m^6A-RIP. m^6A-RIP was performed using an EpiMark N6-Methyladenosine Enrichment Kit (NEB) according to the manufacturer's protocol. The input and precipitated RNAs were purified and reverse-transcribed using a High-Capacity cDNA Reverse Transcription Kit (Thermo Fisher Scientific) and analyzed by RT–qPCR or semi-quantitative RT–PCR as described above.

In vitro pulldown assay

In vitro pulldown assays were performed as previously reported (Yamazaki, Souquere *et al*, 2018; Shibata, Nagano *et al*, 2021). In brief, $(GGAAT)_{20}$, $(GGACT)_{20}$, $(AAGGT)_{20}$, and $(AGGAT)_{20}$ double-strand DNAs were introduced into pCR-Blunt II-TOPO (Thermo Fisher). After restriction enzyme vector linearization, the repeat RNAs were synthesized by *in vitro* transcription using T7 RNA polymerase with NTP mix containing biotinylated UTP and purified using Centri-Sep Spin Columns (Thermo Fisher). For transcription of biotinylated GGm^6Am^6AU repeat RNA, we used m^6ATP instead of ATP. One microgram of *in vitro* transcribed biotinylated RNA was bound to MagCapture HP Tamavidin2-REV magnetic beads (Wako); mixed with pre-absorbed HeLa nuclear extract diluted in PBS containing 0.1% Triton X-100, 1× protease inhibitor, 1 mM PMSF, and RNAse inhibitor; and rotated overnight at 4°C. After washing five times with cold PBS containing 0.1% Triton X-100, the co-precipitated proteins were eluted in SDS sample buffer for 5 min at 95°C.

Gene ontology analysis

Gene ontology (GO) functional enrichment analyses were performed using DAVID Bioinformatics Resources 6.8 (LHRI).

Quantification, statistical analysis, and data plotting

RT–qPCR results were quantified using LightCycler 480 software, version 1.5 (Roche). Semi-quantitative RT–PCR and Western blot results were quantified using ImageJ software (NIH). FISH and IF data were quantified using ImageJ (FIJI) software. The statistical significance of two-group and multiple comparisons was tested using GraphPad Prism7 software (GraphPad Software), as indicated in each figure legend. Non-adjusted (two-group comparison) and adjusted (multiple comparison) *P*-values are indicated in each figure. In box plots, the first and third quartiles are the ends of the box, the median is indicated with a vertical line in the box, and the minimum and maximum except for the outliers are the ends of the whiskers. The outliers are indicated with open circles.

Data availability

The RNA-seq and m^6A-RIP-seg data from this publication have been deposited to the DNA Data Bank of Japan (DDBJ) database [DRA009789 (https://ddbj.nig.ac.jp/DRASearch/submission?acc=DRA009789)] and the Gene Expression Omnibus (GEO) database [GSE164200 (https://www-ncbi-nlm-nih-gov.ezproxy.u-pec.fr/geo/query/acc.cgi?acc=GSE164200)], respectively.

Expanded View for this article is available online.

Acknowledgements
The authors thank Prof. Y. Suzuki (University of Tokyo) for conducting the RNA-seq analysis and the members of the Hirose laboratory for valuable discussions. The computational analysis was partially performed on the NIG supercomputer at the ROIS National Institute of Genetics. This research was supported by JSPS KAKENHI grants nos. 26113002, 16H06279, 17H03630, 17K19335, 19K22374, 20H00448, 20H05377 (to T.H.), 18H05272 (to T.S.), JP19K06478 (to K.N.), and 17H05610, 20H04853 (to S.A.), JST CREST grant no. JPMJCR20E6 (to T.H.), JST ERATO grant no. JPMJER2002 (to T.S.), and the Tokyo Biochemical Research Foundation (to T.H.).

Author contributions
KN and TH conceived and designed the study. KN conducted most of the experiments. YS and TS performed the RNA mass spectrometry analysis. SA and TN performed the peptide-mass spectrometry analyses. MKA supported the FISH-IF and m^6A-RIP-seq experiments. JI, GT, KN, and KA analyzed the bioinformatic data from the RNA-seq. KN and TH wrote the manuscript.

Conflict of interest
The authors declare that they have no conflict of interest.

References

Akichika S, Hirano S, Shichino Y, Suzuki T, Nishimasu H, Ishitani R, Sugita A, Hirose Y, Iwasaki S, Nureki O *et al* (2019) Cap-specific terminal N (6)-methylation of RNA by an RNA polymerase II-associated methyltransferase. *Science* 363: eaav0080

Alarcon CR, Goodarzi H, Lee H, Liu X, Tavazoie S, Tavazoie SF (2015) HNRNPA2B1 is a mediator of m(6)A-dependent nuclear RNA processing events. *Cell* 162: 1299 – 1308

Aly MK, Ninomiya K, Adachi S, Natsume T, Hirose T (2019) Two distinct nuclear stress bodies containing different sets of RNA-binding proteins are formed with HSATIII architectural noncoding RNAs upon thermal stress exposure. *Biochem Biophys Res Commun* 516: 419 – 423

Bi Z, Liu Y, Zhao Y, Yao Y, Wu R, Liu Q, Wang Y, Wang X (2019) A dynamic reversible RNA N(6) -methyladenosine modification: current status and perspectives. *J Cell Physiol* 234: 7948 – 7956

Biamonti G, Vourc'h C (2010) Nuclear stress bodies. *Cold Spring Harb Perspect Biol* 2: a000695

Bokar JA, Shambaugh ME, Polayes D, Matera AG, Rottman FM (1997) Purification and cDNA cloning of the AdoMet-binding subunit of the human mRNA (N6-adenosine)-methyltransferase. *RNA* 3: 1233 – 1247

Delaunay S, Frye M (2019) RNA modifications regulating cell fate in cancer. *Nat Cell Biol* 21: 552 – 559

Dobin A, Davis CA, Schlesinger F, Drenkow J, Zaleski C, Jha S, Batut P, Chaisson M, Gingeras TR (2013) STAR: ultrafast universal RNA-seq aligner. *Bioinformatics* 29: 15 – 21

Dominguez D, Tsai YH, Weatheritt R, Wang Y, Blencowe BJ, Wang Z (2016) An extensive program of periodic alternative splicing linked to cell cycle progression. *Elife*: 5: e10288

Du H, Zhao Y, He J, Zhang Y, Xi H, Liu M, Ma J, Wu L (2016) YTHDF2 destabilizes m(6)A-containing RNA through direct recruitment of the CCR4-NOT deadenylase complex. *Nat Commun* 7: 12626

Frankish A, Diekhans M, Ferreira A-M, Johnson R, Jungreis I, Loveland J, Mudge JM, Sisu C, Wright J, Armstrong J *et al* (2019) GENCODE reference annotation for the human and mouse genomes. *Nucleic Acids Res* 47: D766 – D773

Fustin J-M, Doi M, Yamaguchi Y, Hida H, Nishimura S, Yoshida M, Isagawa T, Morioka M, Kakeya H, Manabe I *et al* (2013) RNA-methylation-dependent RNA processing controls the speed of the circadian clock. *Cell* 155: 793-806

Guil S, Caceres JF (2007) Stressful splicing. *Mol Cell* 28: 180 – 181

Harper JE, Miceli SM, Roberts RJ, Manley JL (1990) Sequence specificity of the human mRNA N6-adenosine methylase *in vitro*. *Nucleic Acids Res* 18: 5735 – 5741

Hessenkemper W, Baniahmad A (2013) Targeting heat shock proteins in prostate cancer. *Curr Med Chem* 20: 2731 – 2740

Hirose T, Yamazaki T, Nakagawa S (2019) Molecular anatomy of the architectural NEAT1 noncoding RNA: The domains, interactors, and biogenesis pathway required to build phase-separated nuclear paraspeckles. *Wiley Interdiscip Rev RNA* 10: e1545

Knuckles P, Buhler M (2018) Adenosine methylation as a molecular imprint defining the fate of RNA. *FEBS Lett* 592: 2845 – 2859

Kopp F, Mendell JT (2018) Functional classification and experimental dissection of long noncoding RNAs. *Cell* 172: 393 – 407

Li A, Chen Y-S, Ping X-L, Yang X, Xiao W, Yang Y, Sun H-Y, Zhu Q, Baidya P, Wang X *et al* (2017) Cytoplasmic m(6)A reader YTHDF3 promotes mRNA translation. *Cell Res* 27: 444 – 447

Liao Y, Smyth GK, Shi W (2014) featureCounts: an efficient general purpose program for assigning sequence reads to genomic features. *Bioinformatics* 30: 923 – 930

Liu J, Yue Y, Han D, Wang X, Fu Ye, Zhang L, Jia G, Yu M, Lu Z, Deng X *et al* (2014) A METTL3-METTL14 complex mediates mammalian nuclear RNA N6-adenosine methylation. *Nat Chem Biol* 10: 93 – 95

Love MI, Huber W, Anders S (2014) Moderated estimation of fold change and dispersion for RNA-seq data with DESeq2. *Genome Biol* 15: 550

Martin M (2011) Cutadapt removes adapter sequences from high-throughput sequencing readsCutadapt removes adapter sequences from high-throughput sequencing reads. *EMBnet.journal* 17: 10 – 12

Metz A, Soret J, Vourc'h C, Tazi J, Jolly C (2004) A key role for stress-induced satellite III transcripts in the relocalization of splicing factors into nuclear stress granules. *J Cell Sci* 117: 4551 – 4558

Moindrot B, Cerase A, Coker H, Masui O, Grijzenhout A, Pintacuda G, Schermelleh L, Nesterova TB, Brockdorff N (2015) A pooled shRNA screen identifies Rbm15, Spen, and Wtap as factors required for Xist RNA-mediated silencing. *Cell Rep* 12: 562 – 572

Ninomiya K, Adachi S, Natsume T, Iwakiri J, Terai G, Asai K, Hirose T (2020) LncRNA-dependent nuclear stress bodies promote intron retention through SR protein phosphorylation. *EMBO J* 39: e102729

Ninomiya K, Hirose T (2020) Short tandem repeat-enriched architectural RNAs in nuclear bodies: functions and associated diseases. *Non-Coding RNA* 6: 6

Patil DP, Chen CK, Pickering BF, Chow A, Jackson C, Guttman M, Jaffrey SR (2016) m(6)A RNA methylation promotes XIST-mediated transcriptional repression. *Nature* 537: 369 – 373

Ping X-L, Sun B-F, Wang Lu, Xiao W, Yang X, Wang W-J, Adhikari S, Shi Y, Lv Y, Chen Y-S *et al* (2014) Mammalian WTAP is a regulatory subunit of the RNA N6-methyladenosine methyltransferase. *Cell Res* 24: 177 – 189

Preußner M, Goldammer G, Neumann A, Haltenhof T, Rautenstrauch P, Muller-McNicoll M, Heyd F (2017) Body temperature cycles control rhythmic alternative splicing in mammals. *Mol Cell* 67: 433 – 446.e4

Sakaguchi Y, Miyauchi K, Kang BI, Suzuki T (2015) Nucleoside analysis by hydrophilic interaction liquid chromatography coupled with mass spectrometry. *Methods Enzymol* 560: 19 – 28

Schibler U, Kelley DE, Perry RP (1977) Comparison of methylated sequences in messenger RNA and heterogeneous nuclear RNA from mouse L cells. *J Mol Biol* 115: 695 – 714

Schwartz S, Mumbach M, Jovanovic M, Wang T, Maciag K, Bushkin G, Mertins P, Ter-Ovanesyan D, Habib N, Cacchiarelli D *et al* (2014) Perturbation of m6A writers reveals two distinct classes of mRNA methylation at internal and 5' sites. *Cell Rep* 8: 284 – 296

Shi H, Wang X, Lu Z, Zhao BS, Ma H, Hsu PJ, Liu C, He C (2017) YTHDF3 facilitates translation and decay of N(6)-methyladenosine-modified RNA. *Cell Res* 27: 315 – 328

Shi H, Wei J, He C (2019) Where, when, and how: context-dependent functions of RNA methylation writers, readers, and erasers. *Mol Cell* 74: 640 – 650

Shibata T, Nagano K, Ueyama M, Ninomiya K, Hirose T, Nagai Y, Ishikawa K, Kawai G, Nakatani K (2021) Small molecule targeting r(UGGAA)n disrupts RNA foci and alleviates disease phenotype in *Drosophila* model. *Nat Commun* 12: 236

Shin Y, Brangwynne CP (2017) Liquid phase condensation in cell physiology and disease. *Science* 357: eaaf4382

Sims D, Ilott NE, Sansom SN, Sudbery IM, Johnson JS, Fawcett KA, Berlanga-Taylor AJ, Luna-Valero S, Ponting CP, Heger A (2014) CGAT: computational genomics analysis toolkit. *Bioinformatics* 30: 1290 – 1291

Sledz P, Jinek M (2016) Structural insights into the molecular mechanism of the m(6)A writer complex. *Elife* 5: e18434

Viphakone N, Sudbery I, Griffith L, Heath CG, Sims D, Wilson SA (2019) Co-transcriptional loading of RNA export factors shapes the human transcriptome. *Mol Cell* 75: 310 – 323.e8

Wang P, Doxtader KA, Nam Y (2016) Structural basis for cooperative function of Mettl3 and Mettl14 methyltransferases. *Mol Cell* 63: 306 – 317

Wang X, Feng J, Xue Y, Guan Z, Zhang D, Liu Z, Gong Z, Wang Q, Huang J, Tang C *et al* (2016) Structural basis of N(6)-adenosine methylation by the METTL3-METTL14 complex. *Nature* 534: 575 – 578

Wang X, Lu Z, Gomez A, Hon GC, Yue Y, Han D, Fu Ye, Parisien M, Dai Q, Jia G *et al* (2014) N6-methyladenosine-dependent regulation of messenger RNA stability. *Nature* 505: 117 – 120

Wang X, Zhao BS, Roundtree IA, Lu Z, Han D, Ma H, Weng X, Chen K, Shi H, He C (2015) N(6)-methyladenosine modulates messenger RNA translation efficiency. *Cell* 161: 1388 – 1399

Wen J, Lv R, Ma H, Shen H, He C, Wang J, Jiao F, Liu H, Yang P, Tan Li *et al* (2018) Zc3h13 regulates nuclear RNA m(6)A methylation and mouse embryonic stem cell self-renewal. *Mol Cell* 69: 1028 – 1038.e6

Xiao W, Adhikari S, Dahal U, Chen Y-S, Hao Y-J, Sun B-F, Sun H-Y, Li A, Ping X-L, Lai W-Y *et al* (2016) Nuclear m(6)A reader YTHDC1 regulates mRNA splicing. *Mol Cell* 61: 507 – 519

Yamazaki T, Nakagawa S, Hirose T (2019) Architectural RNAs for membraneless nuclear body formation. *Cold Spring Harb Symp Quant Biol* 84: 227 – 237

Yamazaki T, Souquere S, Chujo T, Kobelke S, Chong YS, Fox AH, Bond CS, Nakagawa S, Pierron G, Hirose T (2018) Functional domains of NEAT1 architectural lncRNA induce paraspeckle assembly through phase separation. *Mol Cell* 70: 1038 – 1053.e7

Yang Y, Hsu PJ, Chen YS, Yang YG (2018) Dynamic transcriptomic m(6)A decoration: writers, erasers, readers and functions in RNA metabolism. *Cell Res* 28: 616 – 624

Zaccara S, Ries RJ, Jaffrey SR (2019) Reading, writing and erasing mRNA methylation. *Nat Rev Mol Cell Biol* 20: 608 – 624

Zhong S, Li H, Bodi Z, Button J, Vespa L, Herzog M, Fray RG (2008) MTA is an *Arabidopsis* messenger RNA adenosine methylase and interacts with a homolog of a sex-specific splicing factor. *Plant Cell* 20: 1278 – 1288

Zhou J, Wan J, Gao X, Zhang X, Jaffrey SR, Qian SB (2015) Dynamic m(6)A mRNA methylation directs translational control of heat shock response. *Nature* 526: 591 – 594

Zhou KI, Shi H, Lyu R, Wylder AC, Matuszek Z, Pan JN, He C, Parisien M, Pan T (2019) Regulation of co-transcriptional pre-mRNA splicing by m(6)A through the low-complexity protein hnRNPG. *Mol Cell* 76: 70 – 81.e9

